Title
ATG12-ATG3 interacts with Alix to promote late endosome function and basal autophagic flux

Author
Murrow, Lyndsay Marie

Publication Date
2014

Peer reviewed|Thesis/dissertation

ATG12-ATG3 interacts with Alix to promote late endosome function and basal autophagic flux

by

Lyndsay Marie Murrow

DISSERTATION

Submitted in partial satisfaction of the requirements for the degree of

DOCTOR OF PHILOSOPHY

in

Biomedical Sciences

in the

GRADUATE DIVISION

Dedication

This work is dedicated to Jan Hsi Lui, my biggest supporter,

who I am so excited to be marrying next week

ACKNOWLEDGEMENTS

First and foremost, I would like to thank my graduate advisor, Jay Debnath, for his mentorship and support. I am grateful for his confidence in me during times of uncertainty, and for his invaluable big picture guidance. His enthusiasm for research is contagious–I almost always left his office feeling more excited about my project than when I entered.

I would also like to thank my thesis committee members Diane Barber, Eric Verdin, and Ken Nakamura for their time, constructive criticism, and support. Their outside perspective was particularly helpful in strengthening this story. I am especially grateful to my committee chair Diane Barber for her willingness to ask tough questions and for truly caring about my career goals and future success.

I would like to thank all the members of the Debnath lab, past and present, for making every day at work just a little more fun. Their input during lab meetings and informal discussions has helped expand my scientific thinking and has pushed my project forward. I am particularly grateful to Lilliana Radoshevich, whose work initially identified the ATG12-ATG3 conjugate and provided the basis for my thesis project. I would also like to thank Ritu Malhotra for performing the immunoprecipitation/mass spectrometry experiment that identified Alix as a potential ATG12 binding partner. Lastly, I am so grateful to Candia Kenific for her friendship and advice. We joined the Debnath lab as graduate students the same year, and I have been so lucky to be able to discuss ideas every day with someone I respect so much scientifically. I also thank her for being there to listen (even when I got repetitive), for making me laugh when I needed it most, and for being a wonderful travel buddy and friend.

I am incredibly lucky to have such a supportive family, and I am so grateful for my parents Jim and Joan. They instilled a work ethic and self-confidence in me that has been

invaluable to my success as a scientist, and they have been constant sources of support. I would also like to thank my sisters, Lauren and Carrie, for their friendship and encouragement. I have been so lucky to have both of them in San Francisco for the past two years; sandwich Tuesday has become one of my favorite days of the week.

Finally, I would like to thank Jan, who has made my life so much happier over the last six years than I thought possible. He is my biggest source of support, and I aspire daily to be worthy of his unwavering confidence in me.

Contributions to presented work

The work described in this dissertation was done under the direct supervision and guidance of Dr. Jayanta Debnath.

Contents in Chapters 1 and 3 are modified from the following publication:

> Murrow, L. & Debnath, J. Autophagy as a stress-response and quality-control mechanism: implications for cell injury and human disease. *Annual Review of Pathology* **8**, 105 (2013).

Ritu Malhotra performed the immunoprecipitation/mass spectrometry experiment described in Chapter 2, Figure 7B. Lyndsay Murrow performed all other experiments.

ATG12-ATG3 interacts with Alix to promote late endosome function and basal autophagic flux

By Lyndsay Marie Murrow

ABSTRACT

Autophagy is a highly conserved pathway that degrades cytoplasmic components within the lysosome following sequestration in a double-membrane structure called the autophagosome. Autophagy serves as an essential pro-survival stress response pathway induced by a variety of stresses including starvation, hypoxia, and infection. In addition to its role during the stress response, autophagy plays an essential homeostatic role in the cell, promoting basal turnover of long-lived proteins and organelles and performing a "quality control" function by selectively degrading damaged cytoplasmic components.

Two ubiquitin-like conjugations systems are essential for autophagosome formation and elongation. The first attaches the ubiquitin-like molecule ATG12 to its substrate ATG5, and the second attaches LC3 to the lipid phosphatidylethanolamine. Our lab recently identified a novel conjugation between ATG12 and ATG3, the E2-like conjugating enzyme that mediates LC3 lipidation [1]. Surprisingly, although both ATG12 and ATG3 mediate essential steps in the early autophagy pathway, cells lacking ATG12-ATG3 conjugation display normal LC3 lipidation and autophagosome formation following autophagy induction by starvation. However, in full nutrient conditions, cells lacking ATG12-ATG3 have increased numbers of autophagosomes, indicative of either increased autophagosome formation or decreased turnover.

In this study, we more carefully measured the effect of ATG12-ATG3 conjugation on basal autophagy and found that cells lacking ATG12-ATG3 exhibit decreased autolysosome formation under nutrient-rich conditions, perinuclear accumulation of late endosomes, and impaired late endosome function. We identify an interaction between the ATG12-ATG3 conjugate and the ESCRT accessory protein Alix and find that ATG12-ATG3 promotes Alix functions including exosome release and viral budding. Together, these data identify a molecular interaction between the core autophagy and ESCRT-associated machineries and reveal a role for the alternative ATG12-ATG3 conjugate in late endosome function that is independent of canonical autophagy.

Chapter 1 overviews some of the major open areas of research in the autophagy field, including: 1) differential regulation of stress-induced versus basal autophagic flux, 2) identification of non-canonical roles for ATGs, and 3) mechanisms of crosstalk between the autophagy and endosomal trafficking pathways. In Chapter 2, I present data identifying a role for the alternative ATG12-ATG3 conjugation product in basal autophagy and late endosome function. Finally, in Chapter 3 I discuss the broader implications of the ATG12-ATG3 conjugation system for cell biology and its potential therapeutic relevance in neurodegenerative disease.

TABLE OF CONTENTS

LIST OF FIGURES

Chapter 1

Chapter 2

CHAPTER 1

Introduction

Content in this chapter was modified from the following publication:

Murrow, L. & Debnath, J. Autophagy as a stress-response and quality-control mechanism: implications for cell injury and human disease. *Annual Review of Pathology* **8**, 105 (2013).

Macroautophagy is a tightly regulated catabolic pathway important for cellular homeostasis and the cellular response to stress. During autophagy, bulk cytoplasmic components are sequestered in a double membrane structure called the autophagosome; the autophagosome is subsequently trafficked to the lysosome where its outer membrane fuses to the lysosome, leading to degradation of its contents (**Figure 1**) [2, 3].

Autophagy was first identified in mammalian cells by electron microscopy studies in the 1960s, but an understanding of the molecular pathways involved was not achieved until almost thirty years later, following the discovery of the first autophagy genes (ATGs) through landmark genetic screens in yeast. These initial experiments identified a set of highly conserved ATGs that control autophagy, many of which have mammalian orthologues [4]. Further studies have elucidated the molecular pathways that control autophagy in mammalian systems and have revealed the importance of autophagy in both normal physiology and disease [2]. The identification of yeast ATGs and their mammalian homologues has also enabled experimental manipulation of the autophagy pathway and the development of assays for monitoring autophagic activity and flux (**Figure 2**) [5].

Autophagy initiation and membrane nucleation are controlled by the ULK and class III PI3K complexes, which contain the ATG1 orthologue ULK1 and the ATG6 orthologue Beclin 1, respectively (**Figure 1A**) [6]. Downstream of autophagy initiation, several core ATGs function in two ubiquitin-like conjugation systems essential for early autophagosome formation and membrane expansion (**Figure 1B**) [7-9]. In the first, the ubiquitin-like molecule (UBL) ATG12 is activated by the E1-like enzyme ATG7, transferred to the E2-like conjugating enzyme ATG10, and ultimately attached to ATG5 [8, 10, 11]. In the second, the UBL ATG8, or its mammalian orthologue LC3, is conjugated to the lipid phosphatidylethanolamine by ATG7 and the E2-like

enzyme ATG3 [7, 9, 11, 12]. Lipidated LC3 is incorporated in to the growing autophagosome and is used as a marker of autophagy (**Figure 2B-E**). Loss of any of these core ATGs completely ablates autophagosome formation [9]. **Figure 1** further details the molecular functions of the core autophagy machinery.

AUTOPHAGY IN STRESS RESPONSE

Autophagy is an essential pro-survival pathway induced by a wide variety of stresses including nutrient deprivation, growth factor withdrawal, oxidative stress, pathogen infection, and hypoxia [13]. During periods of stress, autophagy maintains cellular biosynthetic capacity and ATP levels by supplying amino acids for de novo protein synthesis and providing substrates for the tricarboxylic acid (TCA) cycle, such as amino acids and free fatty acids [14]. In the mouse, autophagy is upregulated in almost all tissues except the brain following starvation [15]. Mice lacking the essential autophagy genes *Atg5* or *Atg7* (**Figure 1B**) have decreased plasma and tissue amino acid concentrations and die within one day after birth, likely due to nutrient depletion during the neonatal starvation period [16, 17]. Similarly, hematopoietic stem cells upregulate autophagy following starvation in vivo or cytokine withdrawal in primary culture, and blocking autophagy by treatment with the lysosomal inhibitor bafilomycin A or deletion of *Atg12* leads to increased apoptosis in these cells [18].

The importance of autophagy as a pro-survival catabolic pathway has also been demonstrated in cell culture systems. In *Bax/Bak* double knockout cells, which are unable to undergo apoptosis, intact autophagy protects cells from death following prolonged growth factor withdrawal. In growth factor deprived cells, RNAi-mediated ATG7 depletion or treatment with the autophagy inhibitors 3-methyladenine (3-MA) or chloroquine (CQ) (**Figure 1**) leads to cell

death. Supplying autophagy-deficient cells with the TCA cycle substrate methylpyruvate rescues ATP production and cell viability, demonstrating that the catabolic function of autophagy likely mediates cytoprotection [19]. Importantly, self-eating does not protect a cell indefinitely; rather, autophagy functions as a "battery" that buys cells time, allowing them to survive if the stress is resolved in a timely manner. In this context, autophagy is viewed as a salvage mechanism that provides basic components to sustain core metabolic functions during starvation or stress [20].

SIGNALING PATHWAYS THAT CONTROL AUTOPHAGY

Stress-induced autophagy is primarily controlled at two critical nodes: mammalian target of rapamycin (mTOR) and AMP-activated protein kinase (AMPK). TOR was initially identified as a negative regulator of autophagy in yeast and has been corroborated as a major regulator of mammalian autophagy [13]. The Atg1 orthologue ULK1 is a serine/threonine kinase essential for autophagy induction and autophagosome formation. In mammalian cells, under normal nutrient conditions active mTOR phosphorylates ULK1 and sequesters it in a complex with Atg13 and FIP200, inhibiting autophagy [21-23]. Starvation, amino acid deprivation, or growth factor withdrawal inhibit mTOR activity, leading to autophagy induction (**Figure 3A**) [24]. AMPK is a major positive regulator of autophagy that is activated by a high ratio of AMP to ATP [13]. Under conditions of low intracellular energy, AMPK induces autophagy both by phosphorylating ULK1, leading to increased ULK1 kinase activity, and by inhibiting mTORC1 via phosphorylation of Raptor (**Figure 3A)** [21, 25]. Both AMPK and mTOR also control cell growth and metabolism, coupling autophagy to these processes.

Other important stress response pathways that induce autophagy include HIF-1 signaling in response to hypoxia, p53 signaling downstream of DNA damage, and pattern recognition

receptor (PRR) signaling following pathogen infection [13]. The transcription factor HIF-1 is stabilized under hypoxic conditions, leading to induction of a hypoxia-associated gene expression pattern. The BH3-only protein BNIP3 is one major HIF-1 target, and it is essential for autophagy induction following hypoxia. BNIP3 induces autophagy by binding to Bcl-2 and consequently disrupting the inhibitory interaction between Bcl-2 and the mammalian Atg6 orthologue Beclin 1 (**Figure 3B**) [26]. The tumor suppressor p53 is induced by a wide variety of cellular stresses including DNA damage and plays dual roles in autophagy induction. Multiple transcriptional targets of p53 activate autophagy, including BAX and PUMA. On the other hand, cytosolic p53 also has transcription-independent functions, and cytosolic p53 inhibits autophagy [13]. The consequences of this balance between the pro- and anti-autophagic roles of p53 are not well understood. Finally, PRRs recognize molecular patterns associated with different pathogens and induce autophagy following infection [27].

AUTOPHAGY IN CELLULAR HOMEOSTASIS AND QUALITY CONTROL

Although autophagy was initially identified as a cellular response to stress, it has long been recognized that cells exhibit a basal level of autophagy independent of nutrient and stress status. The generation of tissue-specific conditional knockout *Atg5* and *Atg7* mice first revealed the essential role for basal autophagy in the degradation of protein aggregates and damaged organelles. *Atg7*-deficient hepatocytes and pancreatic β cells, *Atg5*-deficient cardiomyocytes, and *Atg5*- or *Atg7*-deficient muscle cells accumulate abnormal mitochondria and ubiquitin-positive protein aggregates and inclusion bodies [17, 28-32]. Ubiquitinated protein aggregates also accumulate in the brains of neuron-specific *Atg5* and *Atg7* knockout mice [33, 34]. Importantly, in *Atg5*-deficient neurons, diffuse ubiquitin positive proteins accumulate before protein aggregates are

observed, supporting the idea that autophagy plays a crucial role in basal protein turnover in addition to degrading damaged or aggregated proteins [33].

Autophagy acts in parallel with the ubiquitin-proteasome system (UPS) as one of the two principal degradation pathways in the cell. Whereas the UPS mainly degrades short-lived proteins, autophagy specializes in the removal of long-lived proteins, and, unlike the UPS, it is uniquely able to degrade whole organelles such as mitochondria, peroxisomes, and endoplasmic reticulum (ER) [35]. Thus, the homeostatic role of autophagy involves both non-selective degradation that supports basal turnover of cytoplasmic components and selective degradation that specifically targets damaged or aggregated organelles and proteins. Selective autophagy serves an essential cellular quality control function in cells [35].

During selective autophagy, adaptor proteins target the autophagy machinery to specific substrates such as protein aggregates, damaged organelles, or intracellular pathogens. The major autophagy adaptors p62, NBR1, NDP52, and optineurin (OPTN) each contain an LC3 interacting region (LIR) and an ubiquitin-binding domain (UBA/UBZ/UBAN) (**Figure 4A**). These adaptors act as scaffolds to mediate recruitment of ubiquitinated cargo into LC3-containing autophagosomes. NBR1 and p62 promote autophagic degradation of protein aggregates; autophagy-deficient cells accumulate ubiquitin-positive aggregates containing both adaptors (**Figure 4B**) [36, 37]. p62 also promotes autophagic targeting of damaged organelles such as mitochondria, and NBR1 is essential for autophagic degradation of peroxisomes [38, 39]. Finally, the more recently identified adaptors NDP52 and optineurin primarily mediate autophagic degradation of ubiquitinated intracellular pathogens [40-42].

Another ubiquitin-binding protein, HDAC6, is important for autophagic clearance of both protein aggregates and mitochondria. In contrast with the classic cargo receptors that directly

interact with components of the autophagy machinery, HDAC6 recruits dynein microtubule motors and actin remodeling machinery to ubiquitinated substrates, promoting transport of ubiquitinated substrates to autophagosomes and leading to enhanced fusion of autophagosomes to lysosomes at these sites (**Figure 4B**) [43, 44]. Loss of HDAC6 leads to accumulation of ubiquitinated protein aggregates and immature early autophagosomes [44]. Since HDAC6 promotes transport of autophagosomes to ubiquitinated cargo as well as autophagosome maturation at these sites, HDAC6 likely controls both selective degradation of protein aggregates and overall levels of basal autophagic flux. In contrast to the well-characterized autophagy adaptors such as p62 that control selective autophagy, the mechanisms that control non-selective basal autophagy remain poorly understood.

Interestingly, although HDAC6 promotes autophagosome maturation under full nutrient, homeostatic conditions, it does not affect starvation-induced autophagy, demonstrating that these two modes of autophagy are differentially regulated [44]. As discussed above, numerous pathways have been identified that control autophagy downstream of diverse cellular stress signals. Far less is known about the mechanisms controlling basal autophagy in the absence of overt stress. Further exploration of the mechanistic differences between these two modes of autophagy remains a major avenue of research in the autophagy field.

NON-CANONICAL FUNCTIONS OF ATGS

Although ATGs are traditionally thought to function solely as autophagy mediators, several recent studies have described functions for ATGs independent of their roles in early autophagosome formation and elongation. Rubinstein et al. recently identified a novel proapoptotic role for free, unconjugated, ATG12. ATG12 binds and negatively regulates

antiapoptotic Bcl-2 family members via a BH3-like motif [45]. Multiple examples of autophagy-independent functions have also been identified for ATGs during the innate immune response. Following infection, the protozoa *Toxoplasma gondii* induces formation of a parasitophorous vacuole that acts as a replication site. ATG5 mediates recruitment of the IFNγ-inducible GTPase IIGP1 to the vacuole, leading to membrane disruption. Surprisingly, this does not involve autophagosome formation, suggesting that this anti-parasitic role of ATG5 is autophagy-independent [46]. Similarly, coronaviruses induce formation of double membrane vesicles (DMVs) that act as sites of replication. In this case, non-lipidated LC3 decorates the DMV surface and is necessary for coronavirus infection; this process occurs independently of ATG7 [47].

Additional studies have identified roles for some ATGs in controlling the later steps of autophagic trafficking [48, 49]. For example, although the canonical role of the principal ATG12 conjugation product ATG12-ATG5 is in early autophagosome formation and elongation (**Figure 1B**), the ATG12-ATG5 conjugate is also recruited by the lysosomal membrane protein TECPR1 to the autolysosome, where it facilitates autophagosome maturation [50]. Similarly, Beclin1 (ATG6 in yeast) plays dual roles in autophagy induction and autolysosome formation. Beclin1 in complex with ATG14L controls autophagosome induction (**Figure 1A**), whereas Beclin1 in complex with Rubicon controls autophagic flux (**Figure 1C**) [51-53].

Although the principal substrate of ATG12 is ATG5, resulting in formation of the ATG12-ATG5 conjugate required for autophagosome formation, our lab recently identified ATG3 as an additional ATG12 conjugation target. Surprisingly, although ATG12 and ATG3 are both core autophagy components, disrupting ATG12 conjugation to ATG3 does not compromise ATG3-mediated LC3 lipidation or starvation-induced autophagy. Rather, cells lacking ATG12-

ATG3 display striking defects in mitochondrial homeostasis, characterized by impaired mitochondrial fusion and reduced targeting of mitochondria to autophagosomes [1].

Interestingly, in our initial studies, we consistently observed increased numbers of autophagosomes in cells lacking ATG12-ATG3 under basal, nutrient-rich conditions, but not during starvation [1]. These findings suggest that loss of ATG12-ATG3 conjugation impacts basal autophagy, either by enhancing autophagosome formation or delaying autophagosome maturation. In Chapter 2, I present work demonstrating that ATG12-ATG3 promotes autolysosome formation under nutrient-rich conditions; moreover, this function is independent from the canonical role of ATG12 or ATG3 in autophagosome formation.

INTERCONNECTIONS BETWEEN THE ESCRT MACHINERY AND AUTOPHAGY

The endosomal sorting complexes required for transport (ESCRT) are a class of proteins required for intralumenal vesicle formation in multivesicular bodies (MVBs) and sorting of endocytosed proteins into this compartment for subsequent lysosomal degradation [54]. Endocytosed material is internalized by budding of the cell membrane towards the cytoplasm and is then trafficked to early endosomes. From there, it can be sent back to the plasma membrane via recycling endosomes. Material that is destined for degradation remains in the early endosome, which matures into a late endosome, also known as an MVB. As the late endosome matures, material is sorted into smaller vesicles that bud off from the endosomal membrane; this process of intralumenal vesicle formation is essential for normal MVB function. Contents in the MVB are degraded following fusion with the lysosome, leading to termination of signaling (**Figure 5**). Protein sorting into MVBs is essential for receptor downregulation and allows the cell to appropriately respond to its external environment [55, 56].

At the late endosome, four complexes mediate intralumenal vesicle formation and sorting of proteins into late endosomes. ESCRT-0, ESCRT-I, and ESCRT-II sequentially bind ubiquitinated cargo at the late endosome membrane. ESCRT-II recruits the ESCRT-III membrane remodeling and abscission machinery, leading to membrane budding and intralumenal vesicle formation. In contrast to the other ESCRT machineries, components of the ESCRT-III machinery primarily exist in an inactive cytosolic form and assemble only transiently at the late endosomal membrane into their active polymeric form [54].

In association with accessory proteins such as the ESCRT-III-associated protein Alix (also known as PDCD6IP), the ESCRT machinery also participates in additional topologically similar membrane budding events involving membrane deformation away from the cytoplasm (**Figure 6**). In a poorly understood process, MVBs can fuse with the plasma membrane rather than with the lysosome, leading to secretion of intralumenal vesicles as exosomes [57, 58]. During exosome biogenesis, Alix forms a complex with the heparan sulphate-containing coreceptor syndecan and the scaffolding protein syntenin, mediating loading of signaling cargo into exosomes and promoting exosome release [59]. Similarly, Alix interacts with viral Gag proteins to recruit the ESCRT-III membrane abscission machinery to sites of viral budding [54, 60].

Intriguingly, recent work indicates that ESCRT function is also required for autophagosome maturation [61-63]. Instead of fusing directly to the lysosome, autophagosomes can fuse to late endosomes; this hybrid MVB, also known as an amphisome, then fuses to the lysosome and its contents are degraded (**Figure 5**) [64, 65]. Autophagosome fusion to late endosomes promotes autophagic flux; loss of essential ESCRT components such as the ESCRT-III subunit CHMP2B or ESCRT-I subunit TSG101 blocks MVB biogenesis and leads to accumulation of immature autophagosomes and ubiquitinated protein aggregates [61-63]. However,

a molecular interaction between the core autophagy machinery and ESCRT components has yet to be established, and the mechanisms that regulate autophagosome maturation via fusion to late endosomes versus direct fusion to lysosomes remain unknown.

In Chapter 2, I present work demonstrating that in addition to defects in basal autophagic flux, cells lacking ATG12-ATG3 conjugation exhibit accumulation of abnormal perinuclear MVBs and defects in late endosome-to-lysosome trafficking. Moreover, we identify an interaction between ATG12-ATG3 and the ESCRT-III-associated protein Alix. Disruption of ATG12-ATG3 conjugation impairs multiple Alix-mediated functions including late endosome distribution, exosome biogenesis, and viral budding. Conversely, Alix deficiency specifically impairs basal autophagy, similarly to ATG12-ATG3. Overall, these results identify the interaction between ATG12-ATG3 and Alix as an interconnection between the autophagy and ESCRT machineries that facilitates basal autophagic flux and multiple Alix-associated activities at the MVB/late endosome.

Figure 1

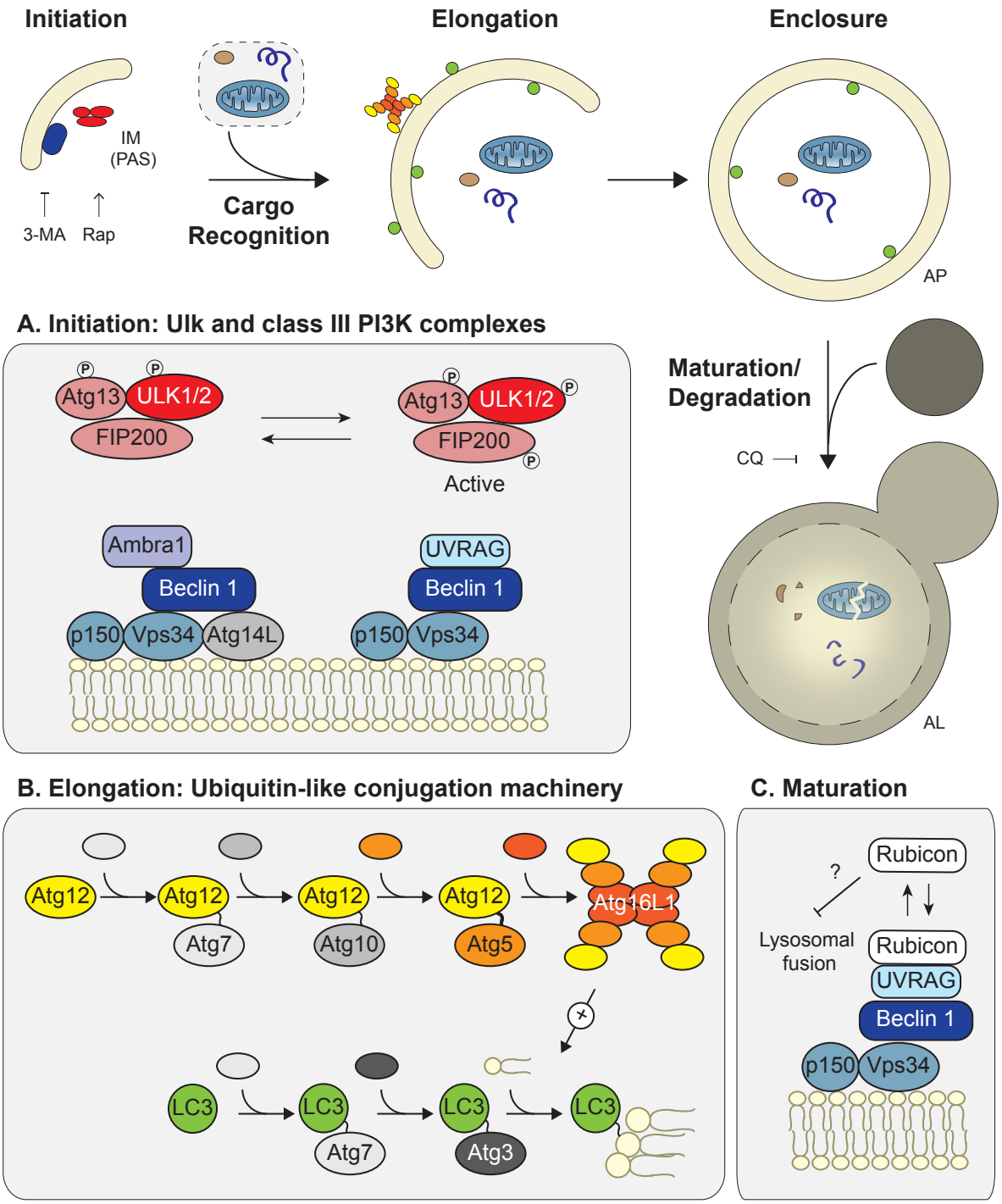
Initiation
Elongation
Enclosure
IM
(PAS)
3-MA
Rap
Cargo
Recognition
AP
A. Initiation: Ulk and class III PI3K complexes
Atg13
ULK1/2
FIP200
Active
Ambra1
Beclin 1
p150
Vps34
Atg14L
UVRAG
Maturation/
Degradation
CQ
AL
B. Elongation: Ubiquitin-like conjugation machinery
Atg12
Atg7
Atg10
Atg5
Atg16L1
LC3
Atg3
C. Maturation
Rubicon
?
Lysosomal
fusion
UVRAG

Figure 1. Overview of the mammalian autophagy machinery

Autophagy occurs in a series of distinct stages: initiation of the isolation membrane (IM, also known as the phagopore assembly site or PAS); cargo recognition; elongation; enclosure of the double-membrane structure to form the autophagosome (AP); and maturation/degradation, in which the AP fuses to the lysosome to form an autolysosome (AL) and its contents are degraded. The autophagy inhibitors 3-methyladenine (3-MA) and chloroquine (CQ) and the autophagy inducer rapamycin (Rap) are shown. **(A)** The ULK and class III PI3K complexes are necessary for autophagy initiation. Beclin 1 forms two distinct autophagy-promoting complexes with the PI3K Vps34. **(B)** The ubiquitin-like conjugation machinery conjugates ATG12 to ATG5 and LC3 to the lipid phosphatidylethanolamine; this machinery mediates autophagosome elongation. Loss of any of these core components (e.g. Beclin 1, ATG5, etc.) leads to autophagy deficiency. **(C)** In addition to its role in autophagy induction, Beclin 1 promotes autophagic maturation via interactions with Rubicon.

Figure 2

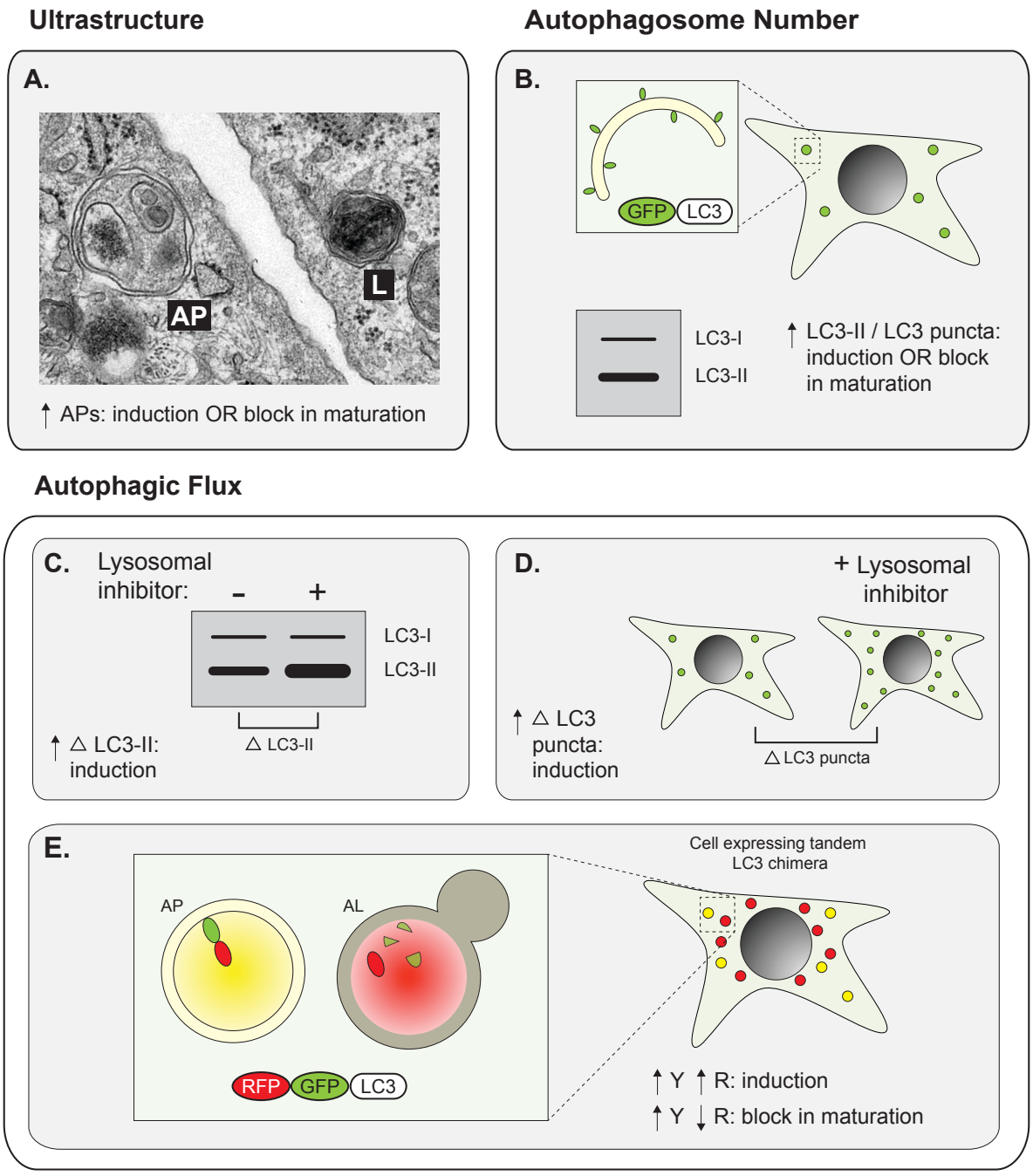
Ultrastructure
Autophagosome Number
A.
AP
L
↑ APs: induction OR block in maturation
B.
GFP
LC3
LC3-I
LC3-II
↑ LC3-II / LC3 puncta: induction OR block in maturation
Autophagic Flux
C.
Lysosomal inhibitor:
-
+
LC3-I
LC3-II
△ LC3-II
↑ △ LC3-II: induction
D.
+ Lysosomal inhibitor
↑ △ LC3 puncta: induction
△ LC3 puncta
E.
AP
AL
RFP
GFP
LC3
Cell expressing tandem LC3 chimera
↑ Y ↑ R: induction
↑ Y ↓ R: block in maturation

Figure 2. Methods for monitoring autophagy

Early studies of autophagy primarily measured total autophagosome number, either **(A)** by identification of APs and ALs by electron microscopy or **(B)** by measuring total levels of lipidated LC3 (LC3-II) or number of LC3 puncta in cells expressing GFP-tagged LC3 (GFP-LC3). Importantly, in both of these cases, an increase in APs can indicate either autophagy induction or a block in AP maturation. Autophagic flux assays more directly measure total autophagic activity. In the presence of lysosomal inhibitors, **(C)** increased accumulation of lipidated LC3 or **(D)** increased accumulation of GFP-LC3 puncta indicates autophagic induction. **(E)** In cells expressing tandem RFP-GFP-tagged LC3, APs are identified as yellow puncta and ALs are detected as red puncta following quenching of GFP fluorescence in the lysosome. An increase in both signals indicates autophagic induction, whereas an increase in yellow with a decrease in red indicates a block in maturation. Abbreviations: AP, autophagosome; AL, autolysosome; LC3-I, unlipidated LC3; LC3-II, lipidated LC3; Δ LC3-II, accumulation of lipidated LC3; Δ LC3 puncta, accumulation of GFP-LC3 puncta; Y, yellow; R, red.

Figure 3

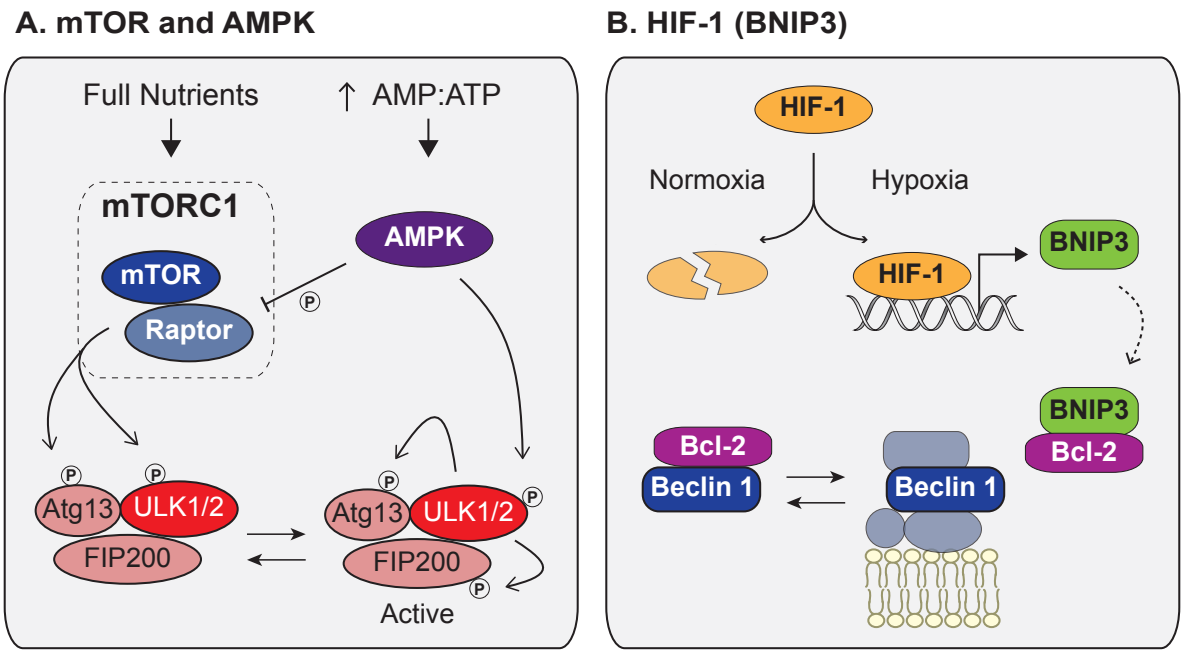

Figure 3. Major stress response pathways that induce autophagy

(A) As part of the mTORC1 complex, active mTOR phosphorylates and inactivates ULK1. Starvation inactivates mTOR, leading to formation of an active ULK1 complex in which ULK1 phosphorylates ATG13 and FIP200. During conditions of low cellular energy, AMPK is activated by high AMP:ATP and induces autophagy both by phosphorylation and activation of ULK1 and by inhibition of mTORC1 via phosphorylation of Raptor. **(B)** HIF-1 and BNIP3 induce autophagy following hypoxia. HIF-1 is stabilized under hypoxic conditions, leading to increased BNIP3 transcription. BNIP3 binds Bcl-2 and disrupts its inhibitory interaction with Beclin 1, leading to autophagy induction.

Figure 4

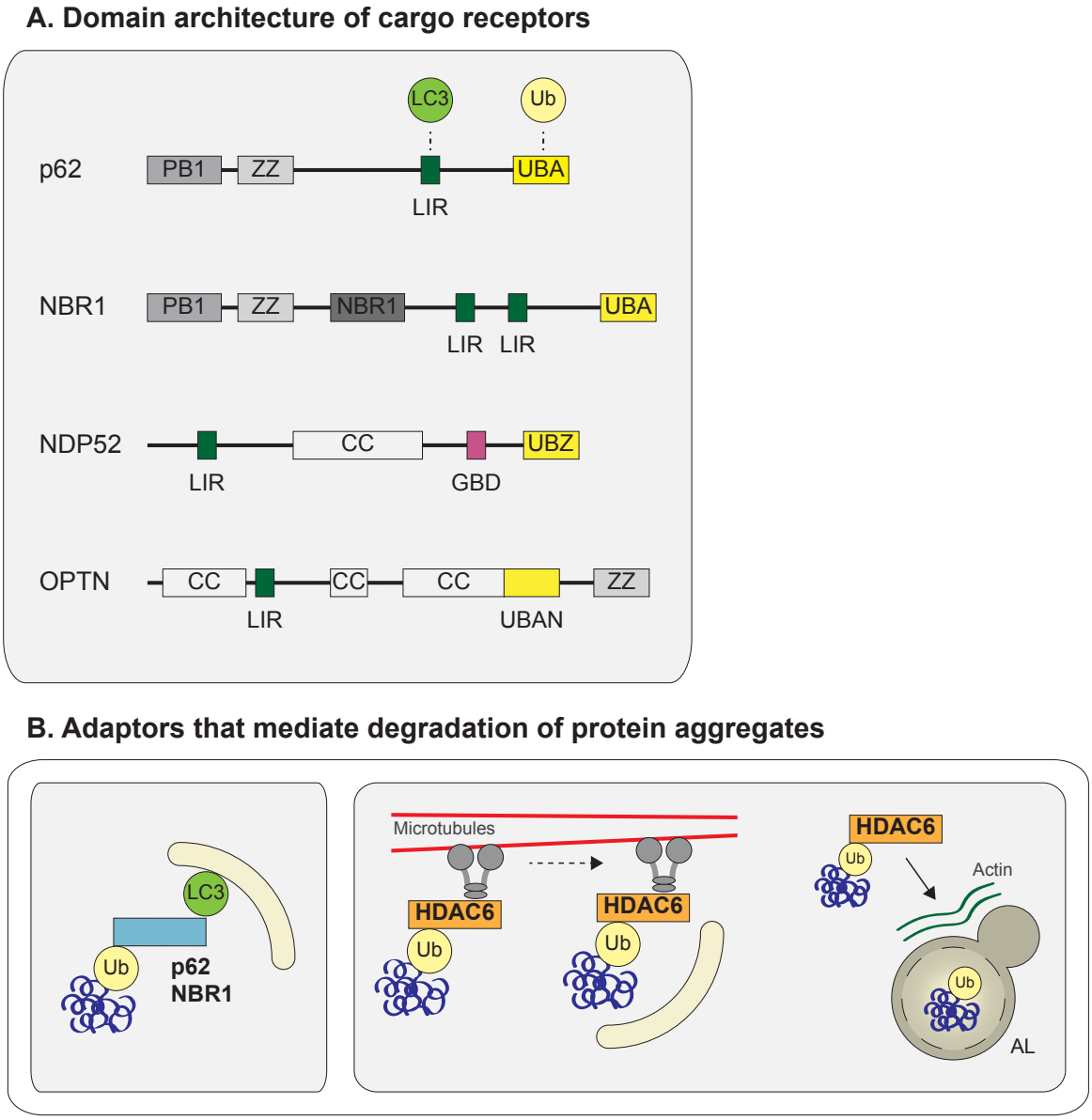
A. Domain architecture of cargo receptors
LC3
Ub
p62
PB1
ZZ
UBA
LIR
NBR1
PB1
ZZ
NBR1
UBA
LIR
LIR
NDP52
CC
UBZ
LIR
GBD
OPTN
CC
CC
CC
ZZ
LIR
UBAN
B. Adaptors that mediate degradation of protein aggregates
LC3
Ub
p62
NBR1
Microtubules
HDAC6
Ub
HDAC6
Ub
HDAC6
Ub
Actin
Ub
AL

Figure 4. Degradation of ubiquitinated autophagy substrates

(**A**) Domain architecture of the autophagy cargo receptors p62, NBR1, NDP52, and optineurin. These autophagy adaptors contain an ubiquitin-binding domain (UBA, UBZ, UBAN) and an LC3-interacting region (LIR), mediating recruitment of LC3-containing APs to ubiquitinated cargo. (**B**) p62 and NBR1 mediate degradation of ubiquitinated protein aggregates via UBA and LIR interactions. HDAC6 is important for clearance of ubiquitinated aggregates and mitochondria. HDAC6 interacts with ubiquitin, dynein motors, and the actin remodeling machinery to promote dynein-mediated transport of ubiquitinated substrates to APs and enhanced AP-lysosome fusion at these sites. Abbreviations: OPTN, optineurin; Ub, ubiquitin.

Figure 5

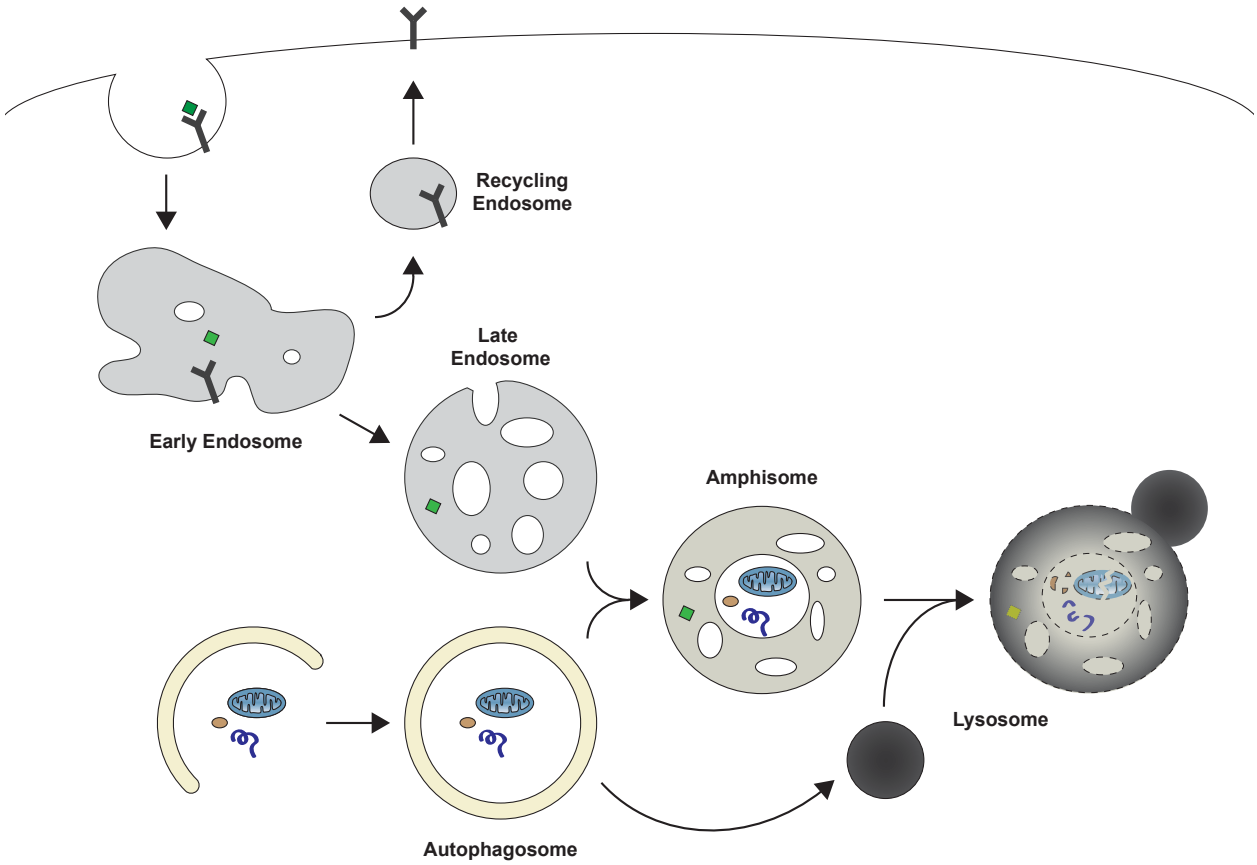

Figure 5. Endocytic trafficking and connections to autophagy

Proteins are endocytosed by internal budding of the cell membrane and trafficked to early endosomes. Material can be sent back to the plasma membrane via recycling endosomes. The early endosome matures into a late endosome, also known as a multivesicular body (MVB). At the late endosome, cargo is sorted into intralumenal vesicles that bud off from the endosomal membrane. Contents are degraded following fusion with the lysosome. Autophagosomes can fuse to late endosomes rather than directly to lysosomes; the resulting hybrid organelle, known as an amphisome, then fuses to the lysosome to form a mature autolysosome.

Figure 6

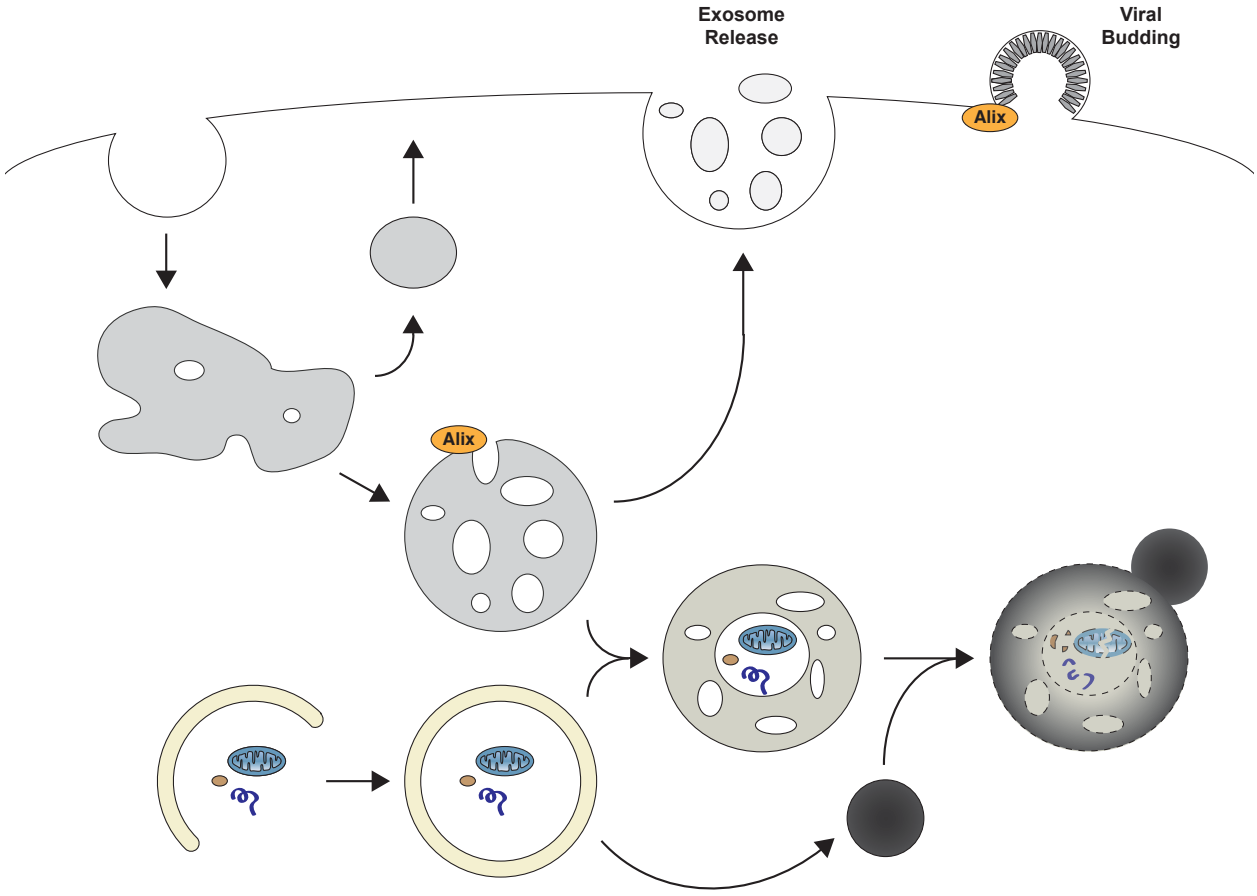

Figure 6. The ESCRT accessory protein Alix mediates additional topologically similar membrane budding events

MVBs can fuse to the plasma membrane rather than to the lysosome, leading to secretion of intralumenal vesicles as exosomes. During exosome biogenesis, Alix forms a complex with exosomal cargo and scaffolding proteins, mediating loading of cargo into exosomes and exosome release. Alix also interacts with viral Gag proteins to at sites of viral budding to promote ESCRT-mediated release of viral particles.

CHAPTER 2

ATG12-ATG3 interacts with Alix to promote late endosome function and basal autophagic flux

SUMMARY

The ubiquitin-like molecule ATG12 is required for the early steps of autophagy. Recently, we identified ATG3, the E2-like enzyme required for ATG8/LC3 lipidation during autophagy, as a novel ATG12 conjugation target. Here, we demonstrate that cells lacking ATG12-ATG3 conjugation have impaired basal autophagic flux, accumulation of perinuclear late endosomes, and impaired endolysosomal trafficking. Furthermore, we identify an interaction between ATG12-ATG3 and the ESCRT-associated protein Alix/PDCD6IP and demonstrate that ATG12-ATG3 controls multiple Alix-dependent processes including late endosome distribution, exosome biogenesis, and viral budding. Lastly, similar to ATG12-ATG3, we show that Alix is functionally required for efficient basal, but not starvation-induced, autophagy. Overall, these results identify a link between the core autophagy and ESCRT machineries and uncover a role for ATG12-ATG3 in late endosome function that is separable from the canonical role of either ATG in autophagosome formation.

HIGHLIGHTS

- Loss of ATG12-ATG3 impedes basal autophagic flux and endolysosomal trafficking.
- ATG12-ATG3 interacts with the ESCRT-associated protein Alix/PDCD6IP.
- ATG12-ATG3 controls Alix functions such as exosome release and viral budding.
- Loss of Alix impairs basal, but not starvation-induced, autophagy.

RESULTS

ATG12-ATG3 conjugation promotes basal autophagic flux

We previously demonstrated that cells lacking ATG12-ATG3 exhibit normal starvation- and rapamycin-induced autophagy, yet, under basal conditions, have significantly increased numbers of autophagosomes [1]. To determine whether this phenotype was due to increased basal autophagosome induction or impaired autophagosome maturation, we used a tandem mCherry-GFP-LC3 reporter. This assay exploits the differing pH sensitivities of GFP and mCherry; GFP is quenched in the acidic lysosomal environment whereas mCherry remains fluorescent [66]. Thus, early autophagosomes correspond to double mCherry/GFP positive puncta whereas mature autolysosomes are marked as mCherry-only puncta (**Chapter 1, Figure 2E**). We reconstituted *Atg3*$^{-/-}$ mouse embryonic fibroblasts (MEFs) with wild-type mouse ATG3 (WTATG3), the K243R mutant of ATG3 (KR) that cannot be conjugated to ATG12, or an empty vector control (pBabe) (**Figure 1A-C**). Importantly, WTATG3 reconstituted *Atg3*$^{-/-}$ MEFs had similar levels of autophagic flux as wild-type *Atg3*$^{+/+}$ MEFs, while no punctate LC3 was observed in *Atg3*$^{-/-}$ MEFs expressing pBabe (**Figure 1D-F**). Consistent with previous results, WTATG3 and KR cells had no significant differences in the percentage of mature autolysosomes following starvation in Hank's buffered saline solution (HBSS) (**Figure 2A, D-E**) [1]. However, when cultured under basal conditions in nutrient-rich media, KR cells exhibited a reduced percentage and total number of mature autolysosomes per cell relative to WTATG3 cells (**Figure 2B, D-E**), indicative of attenuated basal autophagic flux. Notably, KR cells exhibited a reduction, but not complete block, in basal autophagy; upon bafilomycin A (Baf A) treatment to block lysosome acidification, both WTATG3 and KR cells showed further reduced numbers of mature autolysosomes (**Figure 2C-E**). To confirm a defect in basal autophagosome maturation, we

measured protein levels of the autophagy substrate p62 in the detergent-soluble and -insoluble fractions from reconstituted MEFs. KR cells had increased p62 accumulation relative to WTATG3 cells in both fractions (**Figure 2F**). Overall, these results indicate that ATG12-ATG3 specifically promotes basal autophagic flux but does not affect starvation-induced autophagy.

Cells lacking ATG12-ATG3 conjugation accumulate perinuclear late endosomes

To further dissect the defects in autophagosome maturation in cells lacking ATG12-ATG3, we analyzed pBabe, WTATG3, and KR cells by transmission electron microscopy. We observed a striking accumulation of enlarged multivesicular structures in KR cells, corresponding to late endosomes or MVBs (**Figure 3A**). Notably, these vesicles contained cytoplasmic contents and were reminiscent of amphisomes, organelles formed via fusion of autophagosome with endosomes. To more precisely define the organelle alterations in cells lacking ATG12-ATG3, we performed immunostaining for EEA1 to mark early endosomes, lysobisphosphatidic acid (LBPA) to mark late endosomes, and LAMP1 to mark lysosomes. Whereas no obvious changes in the morphology or distribution of early endosomes or lysosomes were seen (**Figure 3B**), a striking difference in late endosome distribution and morphology was observed in cells lacking ATG12-ATG3. In both pBabe and KR cells, MVBs were enlarged and clustered around the nucleus, whereas in WTATG3 cells they were smaller and distributed throughout the cytoplasm (**Figure 3C**). To quantify MVB distribution, we measured the perinuclear $LBPA^+$ fraction, defined as the fraction of LBPA-positive area located within 10 μm of the nucleus (**Figure 3D**). We confirmed a 3-fold increase in the percentage of cells with a perinuclear $LBPA^+$ fraction greater than 0.75 in pBabe and KR cells compared to WTATG3 cells (**Figure 3E**). Hence, ATG12-ATG3 conjugation controls MVB distribution and morphology.

AthTG12-ATG3 promotes late endosome to lysosome trafficking

The endosomal and autophagy pathways are intimately connected; late endosome function is essential for autophagic flux [62]. Since we observed defects in basal autophagosome maturation as well as accumulation of abnormal MVBs in KR cells, we hypothesized that ATG12-ATG3 conjugation was important for trafficking from the late endosomal to the lysosomal compartment. To evaluate endolysosomal trafficking, we used DQ Green BSA (DQ-BSA), a fluorogenic probe that is trafficked through the endosomal pathway and is ultimately dequenched following proteolytic cleavage in the lysosome. We incubated matched wild-type and *Atg3*$^{-/-}$, *Atg12*$^{-/-}$, or *Atg5*$^{-/-}$ MEFs with DQ-BSA, chased for 2h to allow trafficking to the lysosome, and quantified DQ-BSA dequenching by flow cytometry. Intriguingly, *Atg3*$^{-/-}$ and *Atg12*$^{-/-}$ MEFs, which both lack the ATG12-ATG3 conjugate, had decreased DQ-BSA lysosomal degradation. In contrast, *Atg5*$^{-/-}$ MEFs, which lack ATG12-ATG5 but still form ATG12-ATG3, had increased lysosomal degradation (**Figure 4A**). Importantly, all three ATG-deficient lines were autophagy-incompetent, confirmed by their inability to form PE-lipidated LC3 (LC3-II) (**Figure 4B**). Thus, the effects of ATG12 or ATG3 genetic loss on endolysosomal trafficking are separable from the effects of ATG loss on autophagosome formation.

To further define the role of ATG12-ATG3 conjugation in endolysosomal trafficking, we incubated pBabe, WTATG3, and KR cells with fluorescent Bodipy-labeled LDL and immunostained for EEA1, LBPA, and LAMP1 to monitor trafficking kinetics. Following endocytosis, LDL is trafficked from early endosomes into late endosomes and ultimately to lysosomes for degradation. Cells were incubated with LDL and chased for up to 120 min. In WTATG3 cells, LDL was primarily localized to EEA1-positive early endosomes at 0 min, throughout the endocytic pathway at 30 min, and to LBPA- and LAMP1-positive late endosomes

and lysosomes at 120 min (**Figure 5A**). Consistent with a requirement for ATG12-ATG3 in late endosome function, KR cells had significantly decreased trafficking of LDL to the lysosome compared to WTATG3 cells, with a 20% decrease in LDL colocalization with LAMP1 at 120 min (**Figure 4C-D**); Baf A treatment attenuated lysosomal trafficking of LDL in all cell types (**Figure 5B**). Moreover, at this same time point, KR cells had increased colocalization between LDL and LBPA relative to WTATG3 cells (**Figure 4E**), but very little colocalization between LDL and EEA1 (**Figure 5C**), indicative of a specific trafficking block at late rather than early endosomes.

To further assess whether impaired endolysosomal trafficking in KR cells was specific to alterations in late endosome function, we incubated cells with fluorescently labeled transferrin. Transferrin is taken up by receptor-mediated endocytosis, sorted to early endosomes, and trafficked back to the plasma membrane via recycling endosomes. Reconstituted MEFs were incubated with transferrin, chased for up to 60 min, and co-immunostained for EEA1 to mark early endosomes or analyzed by flow cytometry. No differences were observed in either transferrin uptake (0 min chase) or recycling over a 60 min chase period (**Figure 6A-C**), confirming that early endosome function was intact in cells lacking ATG12-ATG3. Additionally, we measured lysosomal mass and acidification using the fluorescent pH indicators LysoSensor Green DND-189 and DND-153. When taken up into lysosomes, LysoSensor DND-189 is fluorescent only in acidic compartments ($pK_a \sim 5.2$) whereas LysoSensor DND-153 is fluorescent at neutral pH ($pK_a \sim 7.5$). Lysosomal content and acidification as measured by flow cytometry was unchanged between pBabe, WTATG3, and KR cells (**Figure 6D**). Finally, we measured lysosomal cathepsin activity with fluorogenic cathepsin B and cathepsin L substrates by flow cytometry. Again, no differences in lysosome function were seen (**Figure 6E**). Thus,

defects in basal autophagic flux and late endosomal trafficking in cells lacking ATG12-ATG3 are not secondary to impaired lysosomal acidification or proteolytic activity; rather, they result from defective trafficking from the late endosomal compartment into lysosomes.

ATG12-ATG3 interacts with the ESCRT-associated protein Alix

To further dissect the role of ATG12-ATG3 in late endosome function, we immunoprecipitated ATG12 from *Atg5*$^{-/-}$ MEFs stably expressing tandem Flag-HA-tagged ATG12 (FHA-ATG12) and subjected the immune complexes to liquid chromatography-tandem mass spectrometry (LC-MS/MS). We identified the ESCRT-associated protein Alix (expected value 7.1×10^{-8}) as a novel interacting protein (**Figure 7A**). Alix associates with multiple components of the ESCRT machinery to control topologically similar membrane events including MVB intralumenal vesicle biogenesis, exosome release, and viral budding [59, 67-70]. To confirm the interaction between Alix and ATG12-ATG3, we transiently expressed WTATG3 or KR in HEK293T cells along with ATG7, ATG12, and Alix. Using this reconstitution system, the ATG12-ATG3 conjugate specifically co-immunoprecipitated with Alix, whereas unconjugated ATG3 from either WTATG3 or KR cells did not (**Figure 7B**). Finally, we confirmed the interaction between Alix and the ATG12-ATG3 conjugate at endogenous protein levels. Alix co-immunoprecipitated with ATG12 in wild-type and *Atg5*$^{-/-}$ MEFs, but not in *Atg3*$^{-/-}$ MEFs which lack the ATG12-ATG3 conjugate (**Figure 7C**).

ATG12-ATG3 conjugation promotes multiple Alix-mediated functions

Given the interaction between ATG12-ATG3 and Alix, we reasoned that defects in late endosome localization and trafficking in KR cells were caused by impaired Alix function.

Previous studies demonstrated that RNAi-mediated Alix depletion results in a perinuclear MVB distribution reminiscent of our results in KR cells [71]. Indeed, we confirmed that Alix knockdown in WTATG3 cells led to perinuclear MVB accumulation similar to that seen in pBabe and KR cells. In contrast, Alix knockdown in pBabe and KR cells did not affect MVB localization, which remained perinuclear (**Figure 8A**).

Based on these results, we hypothesized that ATG12-ATG3 conjugation controls other Alix functions such as exosome release and viral budding. Exosomes are secreted vesicles that play essential signaling roles in a wide variety of processes. They arise when MVBs fuse with the plasma membrane, mediating release of intralumenal vesicles as exosomes [57, 58]. Alix is essential for exosome biogenesis and loading of cargo into exosomal vesicles [59]. Viral budding involves a topologically similar process in which retroviral proteins interact with Alix and other ESCRT proteins to hijack the membrane abscission machinery [54, 60].

To test whether loss of ATG12-ATG3 impaired exosome biogenesis, we isolated exosomal fractions from pBabe, WTATG3, and KR cells by differential high-speed centrifugation. Purified exosomes contained exosomal markers including Alix and TSG101 but were absent of contamination from other membrane sources such as ER and Golgi. Strikingly, both total exosomal protein and specific exosomal marker proteins were decreased in KR versus WTATG3 cells (**Figure 8B**), confirming reduced exosome biogenesis in cells lacking ATG12-ATG3. To measure viral budding, we isolated virus-like particles (VLPs) from cells transfected with YFP-tagged murine leukemia viral Gag protein (MLV Gag-YFP). Since Gag transfection is sufficient for VLP production, this assay allows quantification of viral budding independent of other processes such as infectivity and viral replication. Both Alix and TSG101 interact with the MLV Gag, and loss of either leads to decreased budding of MLV VLPs [69]. Viral budding, as

measured by relative levels of Gag in the VLP fraction, was decreased in pBabe and KR compared to WTATG3 cells (**Figure 8C**). Together, these data demonstrate that ATG12-ATG3 controls multiple Alix-associated functions, including late endosome distribution and trafficking, exosome biogenesis, and viral budding.

Finally, we asked how Alix knockdown affects macroautophagy. Consistent with previous data [72], Alix knockdown did not impact starvation-induced autophagic flux following HBSS treatment as measured by the percentage of mature autolysosomes per cell (**Figure 9A, D**). Rather, Alix knockdown specifically impaired basal autophagic flux in cells grown in nutrient-rich, full media conditions (**Figure 9B, D**). Similar to loss of ATG12-ATG3, Alix depletion led to a reduction, but not complete block, in basal autophagy, as Baf A treatment led to further reduction in autolysosomes (**Figure 9C-D**). Overall, these results uncover an interaction between ATG12-ATG3 and Alix that promotes endolysosomal trafficking, exosome release, viral budding, and basal autophagy.

Figure 1

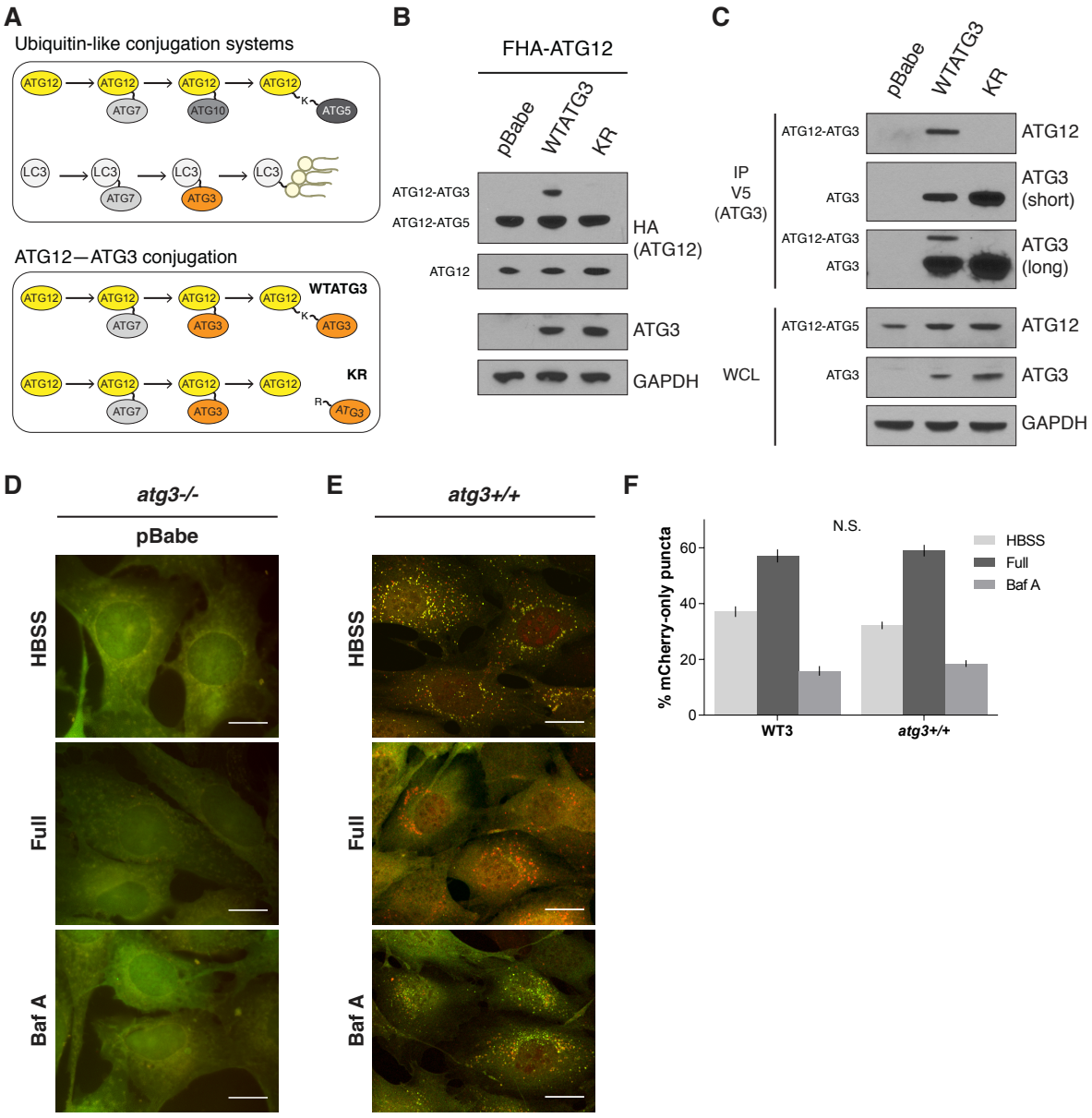
A
Ubiquitin-like conjugation systems
ATG12
ATG7
ATG10
ATG5
LC3
ATG3
ATG12—ATG3 conjugation
WTATG3
KR
B
FHA-ATG12
pBabe
WTATG3
KR
ATG12-ATG3
ATG12-ATG5
ATG12
HA (ATG12)
ATG3
GAPDH
C
IP V5 (ATG3)
WCL
ATG3 (short)
ATG3 (long)
D
atg3-/-
pBabe
HBSS
Full
Baf A
E
atg3+/+
F
N.S.
% mCherry-only puncta
HBSS
Full
Baf A
WT3
atg3+/+

Figure 1. Generation of pBABE, WTATG3, and KR cells and analysis of mCherry-GFP-LC3 in *Atg3*$^{+/+}$ and *Atg3*$^{-/-}$ MEFs

(A) Overview of the ubiquitin-like conjugation systems required for autophagy and formation of the ATG12-ATG3 conjugate. ATG12 is conjugated to lysine 243 (K243) of ATG3. **(B)** Stable pools of *Atg3*$^{-/-}$ MEFs expressing an empty vector control (pBabe), wild-type mouse ATG3 (WTATG3) or the ATG3 K243R (KR) mutant were transduced with Flag-HA-ATG12 (FHA-ATG12). Lysates were immunoblotted for α-HA to detect ATG12 conjugates. **(C)** Lysates from stable pools of *Atg3*$^{-/-}$ MEFs expressing an empty vector control (pBabe), V5-tagged wild-type mouse ATG3 (WTATG3) or V5-tagged mutant K243R ATG3 (KR) were immunoprecipitated with anti-V5. Immune complexes (IP V5) were resolved by SDS-PAGE and immunoblotted with α-ATG3 and α-ATG12 to detect the ATG12-ATG3 conjugate. **(D)** *Atg3*$^{-/-}$ MEFs expressing mCherry-GFP-LC3 were grown in full media (Full), starved in Hank's buffered saline solution (HBSS) for 2h, or treated with bafilomycin A (Baf A, 50 nM). Scale bar, 20 μm. **(E)** *Atg3*$^{+/+}$ MEFs expressing mCherry-GFP-LC3 were grown in full media (Full), HBSS starved for 2h, or treated with Baf A (50 nM). Scale bar, 20 μm. **(F)** Quantification of the percentage of mature autolysosomes, delineated as mCherry-positive, GFP-negative (mCherry-only) puncta, for at least 200 cells from three independent experiments as described in E. Data for WTATG3 cells is the same as that presented in Figure 2D. Data are presented as mean ± SEM. Statistical significance calculated using ANOVA, followed by Tukey's HSD test.

Figure 2

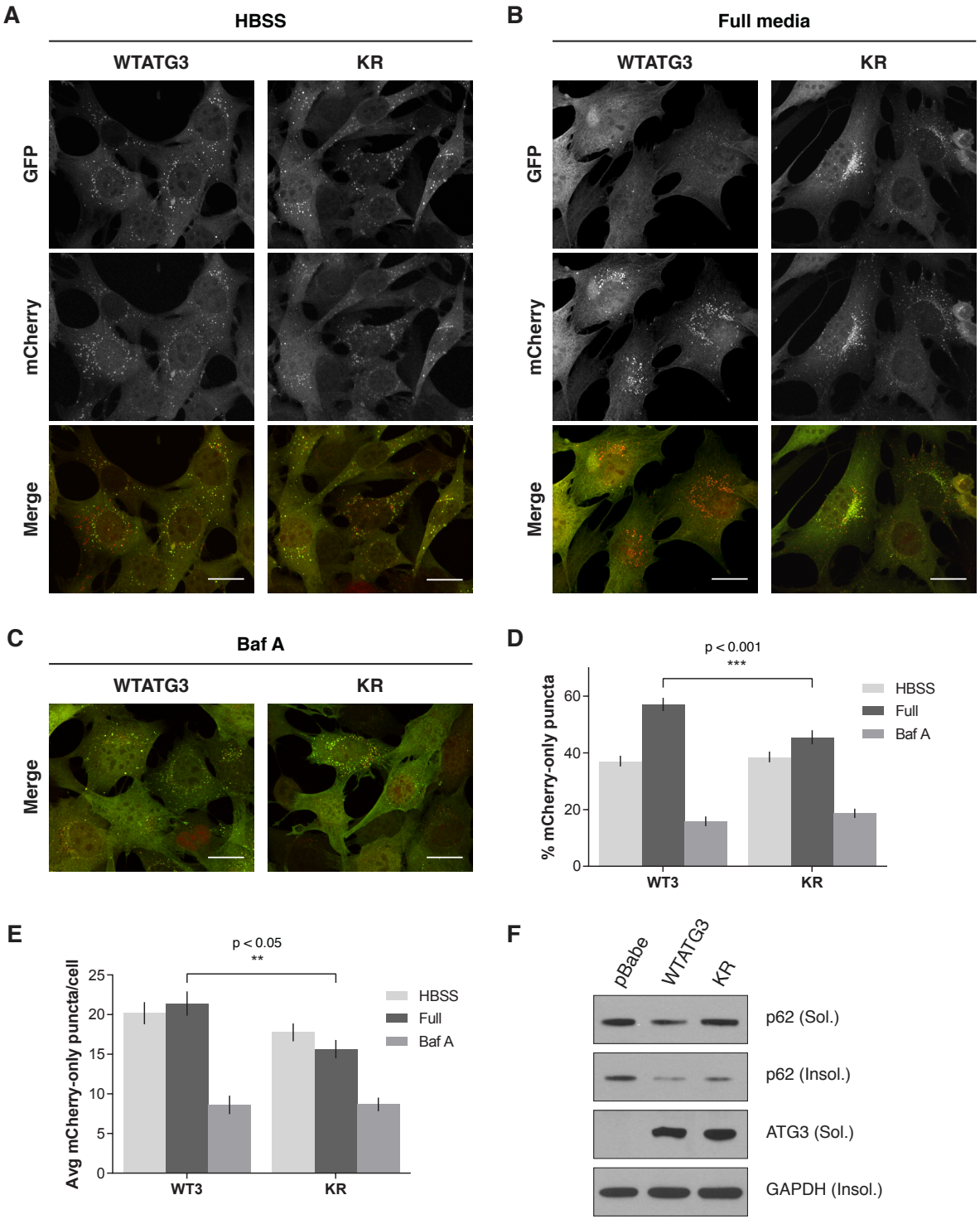
A
HBSS
WTATG3
KR
GFP
mCherry
Merge
B
Full media
WTATG3
KR
GFP
mCherry
Merge
C
Baf A
WTATG3
KR
Merge
D
p < 0.001
***
% mCherry-only puncta
60
40
20
0
WT3
KR
HBSS
Full
Baf A
E
p < 0.05
**
Avg mCherry-only puncta/cell
25
20
15
10
5
0
WT3
KR
HBSS
Full
Baf A
F
pBabe
WTATG3
KR
p62 (Sol.)
p62 (Insol.)
ATG3 (Sol.)
GAPDH (Insol.)

Figure 2. ATG12-ATG3 conjugation promotes basal autophagic flux.

Stable pools of *Atg3*$^{-/-}$ MEFs expressing an empty vector control (pBabe), wild-type mouse ATG3 (WTATG3) or the ATG3 K243R mutant unable to be conjugated to ATG12 (KR) were used for experiments as indicated. **(A)** Indicated cell types expressing mCherry-GFP-LC3 were HBSS starved for 2h to measure starvation-induced autophagic flux. Scale bar, 20 μm. **(B)** Indicated cell types expressing mCherry-GFP-LC3 were grown in full media to measure basal autophagic flux. Scale bar, 20 μm. **(C)** Indicated cell types expressing mCherry-GFP-LC3 were treated for 2h with bafilomycin A (Baf A, 50 nM) to block lysosome function. Scale bar, 20 μm. **(D)** Quantification of the percentage of mCherry-positive, GFP-negative (mCherry-only) puncta per cell for at least 200 cells from three independent experiments as described in A-C (mean ± SEM). Statistical significance calculated using ANOVA, followed by Tukey's HSD test. **(E)** Quantification of the number of mCherry-only puncta per cell for at least 200 cells from three independent experiments as described in A-C (mean ± SEM). Statistical significance calculated using ANOVA, followed by Tukey's HSD test. **(F)** Indicated cell types were lysed in 1% Triton X-100, and triton-soluble (Sol.) and insoluble (Insol.) fractions were immunoblotted with α-p62, α-GAPDH and α-ATG3.

Figure 3

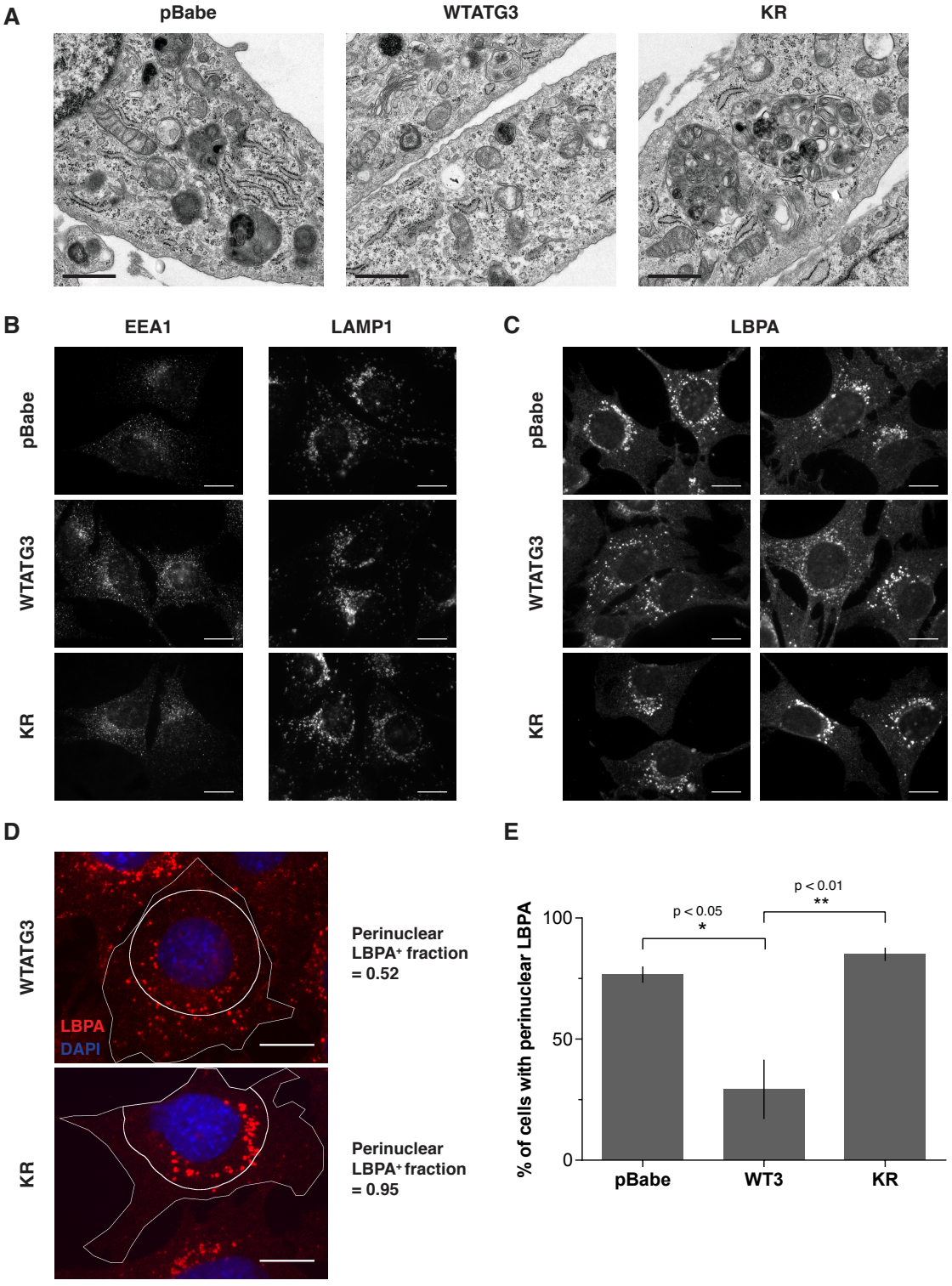
A
pBabe
WTATG3
KR
B
EEA1
LAMP1
pBabe
WTATG3
KR
C
LBPA
pBabe
WTATG3
KR
D
WTATG3
LBPA
DAPI
Perinuclear LBPA+ fraction = 0.52
KR
Perinuclear LBPA+ fraction = 0.95
E
p < 0.05
*
p < 0.01
**
% of cells with perinuclear LBPA
100
50
0
pBabe
WT3
KR

Figure 3. Cells lacking ATG12-ATG3 conjugation accumulate enlarged perinuclear late endosomes.

(A) Indicated cell types were analyzed by transmission electron microscopy. Scale bar, 1 μm. **(B)** Indicated cell types were immunostained with α-EEA1 or α-LAMP1 to mark early endosomes and lysosomes, respectively. Scale bar, 10 μm. **(C)** Indicated cell types were immunostained with α-lysobisphosphatidic acid (LBPA) to mark late endosomes. Scale bar, 10 μm. **(D)** Indicated cell types were immunostained with α-LBPA and DAPI. The perinuclear $LBPA^{+}$ fraction was defined as the fraction of LBPA area located within 10 μm of the nucleus. Scale bar, 10 μm. **(E)** Quantification of the percentage of cells with perinuclear LBPA fraction ≥ 0.75 (mean ± SEM) for 60 cells from three independent experiments as described in D. Statistical significance calculated using ANOVA, followed by Tukey's HSD test.

Figure 4

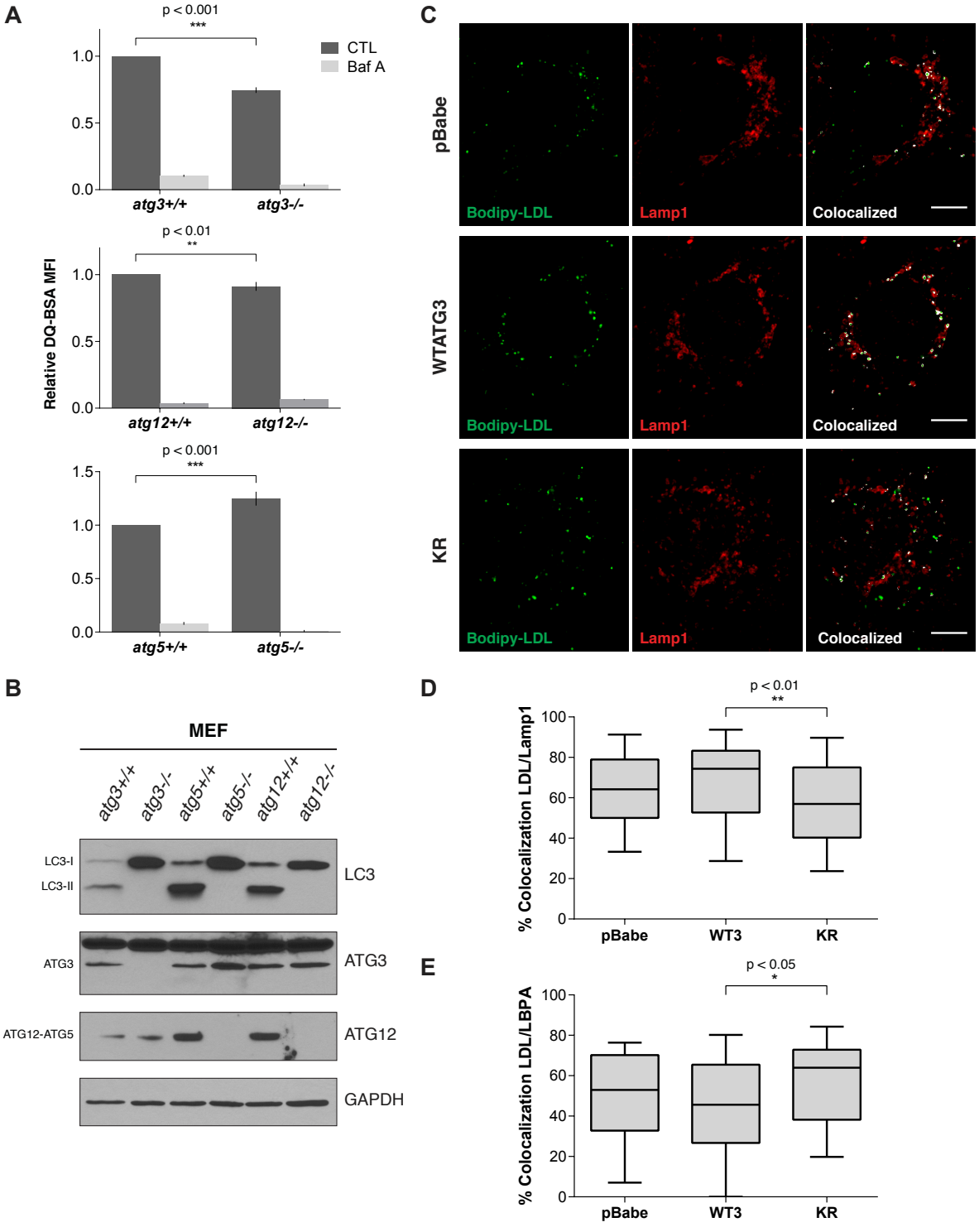
A
p < 0.001
***
CTL
Baf A
1.0
0.5
0.0
atg3+/+
atg3-/-
p < 0.01
**
Relative DQ-BSA MFI
atg12+/+
atg12-/-
p < 0.001
***
1.5
atg5+/+
atg5-/-
C
pBabe
WTATG3
KR
Bodipy-LDL
Lamp1
Colocalized
B
MEF
atg3+/+
atg3-/-
atg5+/+
atg5-/-
atg12+/+
atg12-/-
LC3-I
LC3-II
LC3
ATG3
ATG12-ATG5
ATG12
GAPDH
D
p < 0.01
**
% Colocalization LDL/Lamp1
100
80
60
40
20
0
pBabe
WT3
KR
E
p < 0.05
*
% Colocalization LDL/LBPA

Figure 4. ATG12-ATG3 conjugation promotes late endosome to lysosome trafficking.

(A) Matched wild-type and *Atg*-deficient MEFs as indicated were incubated with DQ-BSA for 30 min at 37°C followed by a 2h chase in full media. Lysosomal degradation as measured by DQ-BSA dequenching was analyzed by flow cytometry. When indicated, Baf A (50 nM) was used during the pulse/chase to block lysosome function. Data are presented as mean ± SEM relative fluorescence intensity from at least three independent experiments. Statistical significance calculated using unpaired two-tailed t test **(B)** Indicated cell types were lysed and immunoblotted with α-LC3, α-ATG3, and α-ATG12. **(C)** Stable pools of reconstituted *Atg3*$^{-/-}$ MEFs were incubated with Bodipy-LDL for 15 min at 37°C followed by a 2h chase in full media. Cells were immunostained with α-LAMP1 to mark lysosomes. Colocalized pixels were highlighted in white using the Colocalization plugin in ImageJ. Scale bar, 5 μm. **(D)** Quantification of the percentage of LDL puncta colocalized with LAMP1 for at least 100 cells from three independent experiments as described in C. Data are presented as median (horizontal line), interquartile range (box), and 10-90th percentile (whiskers). Statistical significance calculated using ANOVA, followed by Tukey's HSD test. **(E)** Quantification of the percentage of LDL puncta colocalized with LBPA for at least 45 cells from three independent experiments. Indicated cell types were incubated with Bodipy-LDL as in C and immunostained with α-LBPA to mark late endosomes. Data are presented as median, interquartile range, and 10-90th percentile. Statistical significance calculated using ANOVA, followed by Tukey's HSD test.

Figure 5

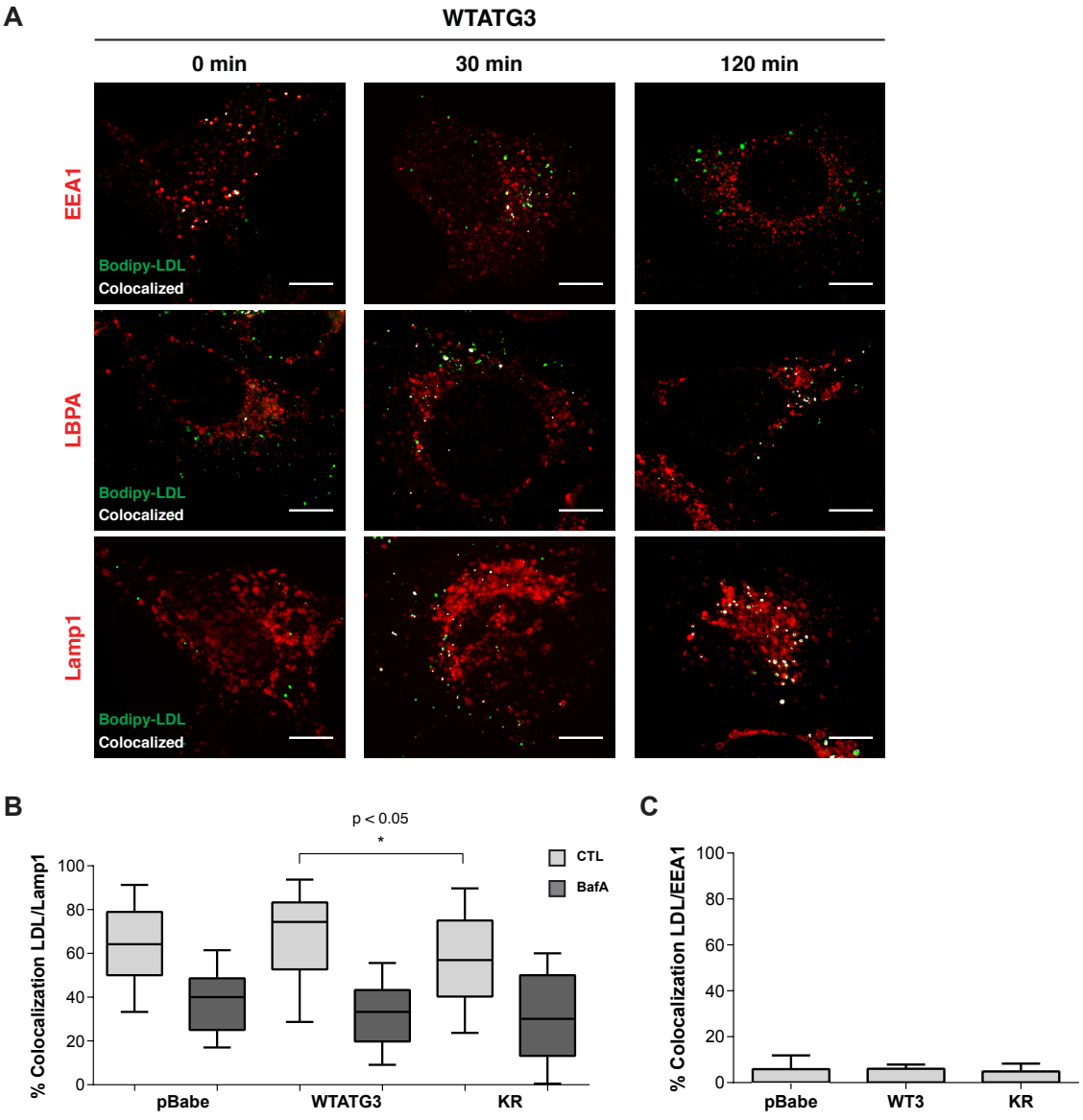
A
WTATG3
0 min
30 min
120 min
EEA1
LBPA
Lamp1
Bodipy-LDL
Colocalized
B
p < 0.05
*
CTL
BafA
% Colocalization LDL/Lamp1
100
80
60
40
20
0
pBabe
WTATG3
KR
C
% Colocalization LDL/EEA1
100
80
60
40
20
0
pBabe
WT3
KR

Figure 5. Endolysosomal trafficking of Bodipy-LDL

Stable pools of *Atg3*$^{-/-}$ MEFs expressing an empty vector control (pBabe), wild-type mouse ATG3 (WTATG3) or the ATG3 KR mutant were used for experiments as indicated. **(A)** *Atg3*$^{-/-}$ MEFs stably expressing wild-type mouse ATG3 (WTATG3) were incubated with Bodipy-LDL for 15 min at 37°C in serum-free media followed by a chase in full media for the indicated times. Cells were immunostained with α-EEA1 to mark early endosomes, α-lysobisphosphatidic acid (LBPA) to mark late endosomes, and α-LAMP1 to mark lysosomes. Colocalized pixels are highlighted in white using the Colocalization plugin in ImageJ. Scale bar, 5 μm. **(B)** Indicated cell types were incubated with Bodipy-LDL for 15 min at 37°C in serum-free media followed by a 2h chase in full media. When indicated, Baf A (50 nM) was used during the chase to block lysosome function. Quantification of the percentage of LDL puncta colocalized with LAMP1 for at least 30 cells is shown. Data for untreated cells (CTL) is the same as Figure 4D. Data are presented as median (horizontal line), interquartile range (box), and 10-90th percentile (whiskers). Statistical significance calculated using ANOVA, followed by Tukey's HSD test. **(C)** Indicated cell types were incubated with Bodipy-LDL for 15 min at 37°C in serum-free media followed by a 2h chase in full media. Cells were immunostained with α-EEA1 to mark early endosomes. Quantification of the percentage of LDL puncta colocalized with EEA1 for at least 30 cells is shown. Data are presented as interquartile range (box) and 90th percentile (whiskers).

Figure 6

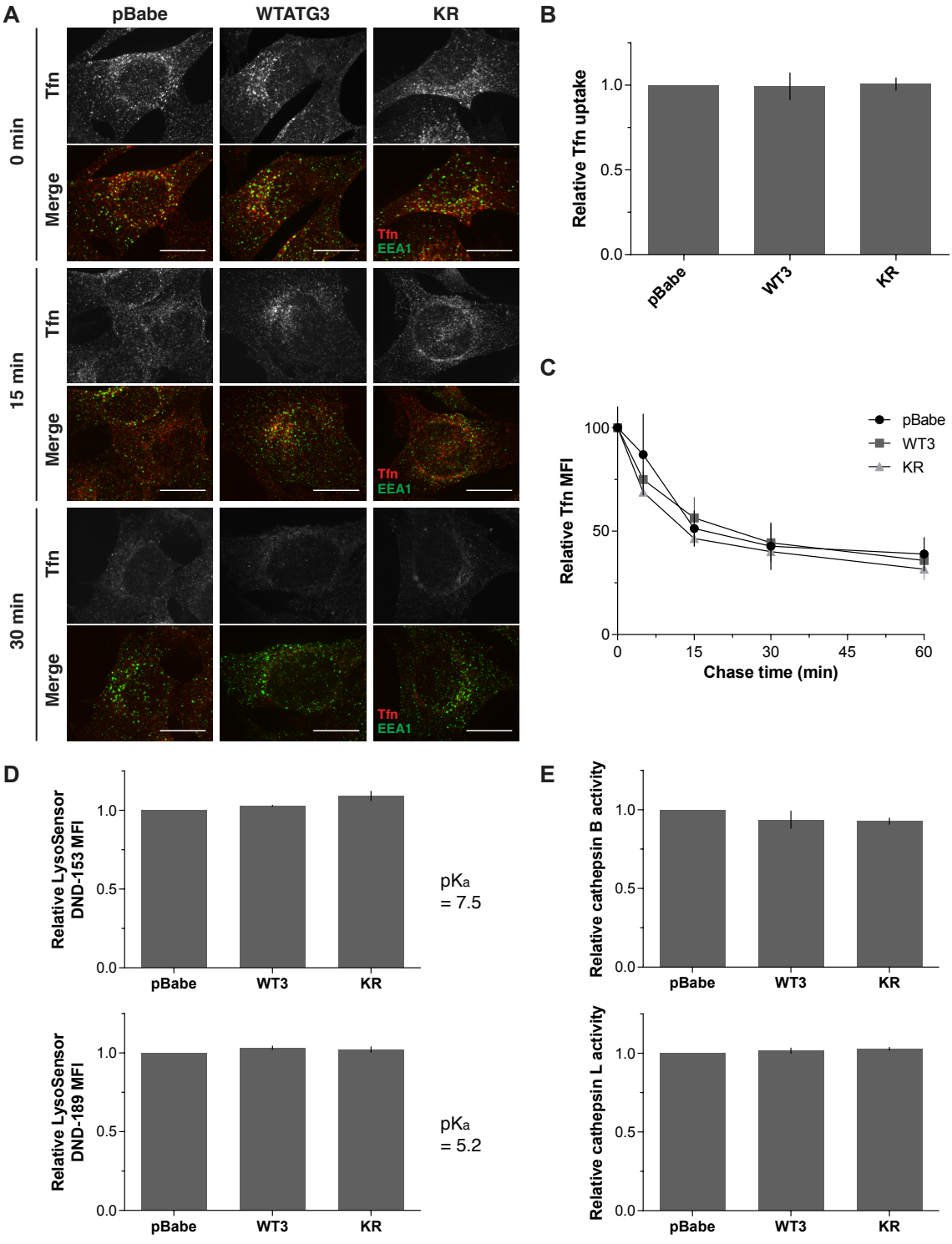
A
pBabe
WTATG3
KR
0 min
15 min
30 min
Tfn
Merge
Tfn
EEA1
B
Relative Tfn uptake
1.0
0.5
0.0
pBabe
WT3
KR
C
Relative Tfn MFI
100
50
0
0
15
30
45
60
Chase time (min)
pBabe
WT3
KR
D
Relative LysoSensor DND-153 MFI
pKa = 7.5
Relative LysoSensor DND-189 MFI
pKa = 5.2
E
Relative cathepsin B activity
Relative cathepsin L activity

Figure 6. ATG12-ATG3 conjugation does not affect early endosome or lysosome function.

(A) Indicated cell types were incubated with fluorescently labeled transferrin (Tfn, red) for 15 min at 37°C in serum-free media followed by a chase in full media for the indicated times. Cells were immunostained for EEA1 (green) to mark early endosomes. Scale bar, 10 μm. **(B)** Indicated cell types were incubated with Tfn as in A. Cells were fixed immediately following pulse and Tfn uptake was measured by flow cytometry. Data are presented as mean ± SEM relative fluorescence intensity from three independent experiments. **(C)** Indicated cell types were incubated with Tfn as in A and chased in full media for the indicated times. Tfn recycling as measured by a decrease in fluorescence over time was quantified by flow cytometry. Data are presented as mean ± SEM relative fluorescence intensity from three independent experiments. **(D)** Indicated cell types were incubated with LysoSensor DND-153 or DND-189 to measure total or acidic (pH < 5.2) lysosomal content, respectively. Data is presented as mean ± SEM relative fluorescence intensity from three independent experiments. **(E)** Indicated cell types were incubated with fluorogenic Magic Red cathepsin B or cathepsin L substrates to measure cathepsin activity. Data is presented as mean ± SEM relative fluorescence intensity from three independent experiments.

Figure 7

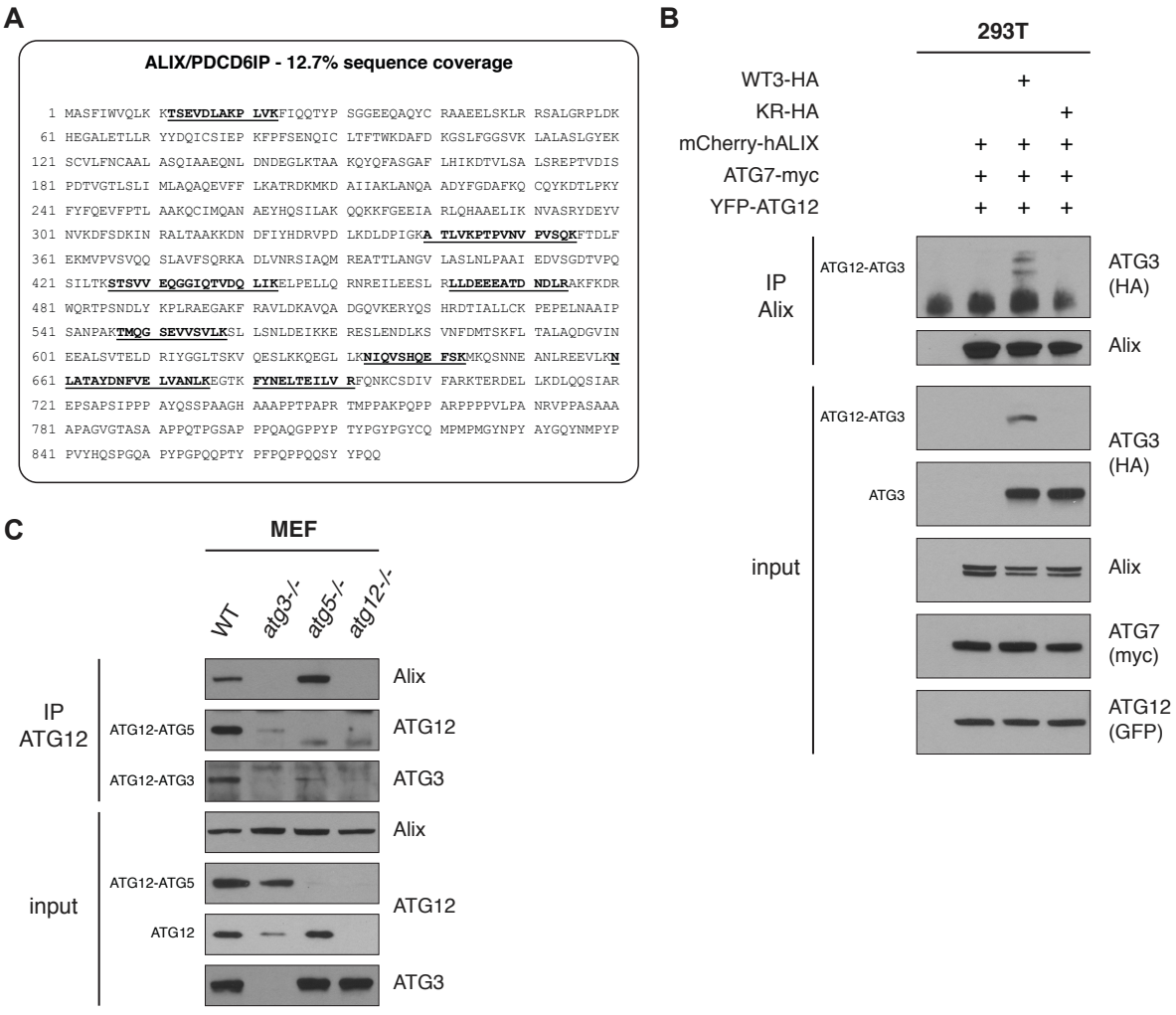
A
ALIX/PDCD6IP - 12.7% sequence coverage
1 MASFIWVQLK KTSEVDLAKP LVKFIQQTYP SGGEEQAQYC RAAEELSKLR RSALGRPLDK
61 HEGALETLLR YYDQICSIEP KFPFSENQIC LTFTWKDAFD KGSLFGGSVK LALASLGYEK
121 SCVLFNCAAL ASQIAAEQNL DNDEGLKTAA KQYQFASGAF LHIKDTVLSA LSREPTVDIS
181 PDTVGTLSLI MLAQAQEVFF LKATRDKMKD AIIAKLANQA ADYFGDAFKQ CQYKDTLPKY
241 FYFQEVFPTL AAKQCIMQAN AEYHQSILAK QQKKFGEEIA RLQHAAELIK NVASRYDEYV
301 NVKDFSDKIN RALTAAKKDN DFIYHDRVPD LKDLDPIGKA TLVKPTPVNV PVSQKFTDLF
361 EKMVPVSVQQ SLAVFSQRKA DLVNRSIAQM REATTLANGV LASLNLPAAI EDVSGDTVPQ
421 SILTKSTSVV EQGGIQTVDQ LIKELPELLQ RNREILEESL RLLDEEEATD NDLRAKFKDR
481 WQRTPSNDLY KPLRAEGAKF RAVLDKAVQA DGQVKERYQS HRDTIALLCK PEPELNAAIP
541 SANPAKTMQG SEVVSVLKSL LSNLDEIKKE RESLENDLKS VNFDMTSKFL TALAQDGVIN
601 EEALSVTELD RIYGGLTSKV QESLKKQEGL LKNIQVSHQE FSKMKQSNNE ANLREEVLKN
661 LATAYDNFVE LVANLKEGTK FYNELTEILV RFQNKCSDIV FARKTERDEL LKDLQQSIAR
721 EPSAPSIPPP AYQSSPAAGH AAAPPTPAPR TMPPAKPQPP ARPPPPVLPA NRVPPASAAA
781 APAGVGTASA APPQTPGSAP PPQAQGPPYP TYPGYPGYCQ MPMPMGYNPY AYGQYNMPYP
841 PVYHQSPGQA PYPGPQQPTY PFPQPPQQSY YPQQ
B
293T
WT3-HA
KR-HA
mCherry-hALIX
ATG7-myc
YFP-ATG12
IP Alix
ATG12-ATG3
ATG3 (HA)
Alix
input
ATG12-ATG3
ATG3 (HA)
ATG3
Alix
ATG7 (myc)
ATG12 (GFP)
C
MEF
WT
atg3-/-
atg5-/-
atg12-/-
IP ATG12
ATG12-ATG5
ATG12-ATG3
Alix
ATG12
ATG3
input
ATG12-ATG5
ATG12
Alix
ATG12
ATG3

Figure 7. ATG12-ATG3 interacts with Alix/PDCD6IP.

(A) ATG12 was immunoprecipitated from *Atg5*$^{-/-}$ MEFs stably expressing tandem tagged Flag-HA-ATG12. Eluted proteins were resolved by SDS-PAGE, and Coomassie-stained protein bands were subject to LC-MS/MS analysis. Alix/PDCD6IP was identified; bold underlined sequences correspond to independent peptides identified by mass spectrometry. **(B)** HEK293T cells were transfected with mCherry-hALIX, Myc-tagged ATG7, YFP-ATG12, and HA-tagged wild-type ATG3 (WTATG3-HA) or mutant K243R ATG3 (KR-HA) as indicated. Lysates were immunoprecipitated with α-Alix. Immune complexes (IP Alix) were resolved by SDS-PAGE and immunoblotted with α-HA and α-Alix. **(C)** MEFs with the indicated genotypes were lysed and immunoprecipitated with α-ATG12. Immune complexes (IP ATG12) were resolved by SDS-PAGE and immunoblotted with α-Alix, α-ATG12, and α-ATG3.

Figure 8

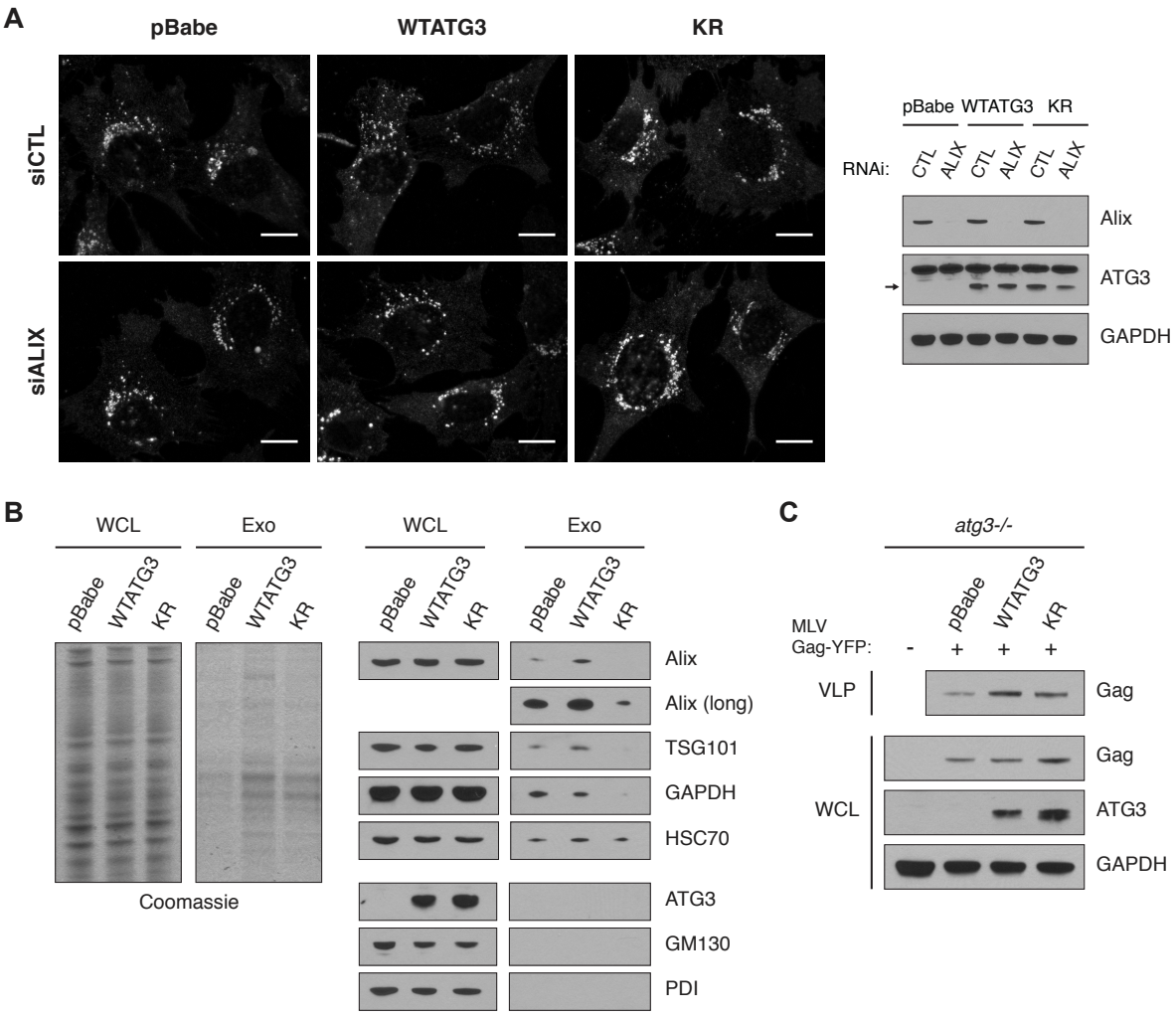
A
pBabe
WTATG3
KR
siCTL
siALIX
pBabe WTATG3 KR
RNAi: CTL ALIX CTL ALIX CTL ALIX
Alix
ATG3
GAPDH
B
WCL
Exo
WCL
Exo
pBabe WTATG3 KR pBabe WTATG3 KR pBabe WTATG3 KR pBabe WTATG3 KR
Alix
Alix (long)
TSG101
GAPDH
HSC70
ATG3
GM130
PDI
Coomassie
C
atg3-/-
pBabe WTATG3 KR
MLV Gag-YFP: - + + +
VLP
Gag
WCL
Gag
ATG3
GAPDH

Figure 8. Loss of ATG12-ATG3 conjugation phenocopies defects in Alix function.

(A) Indicated cell types were transfected with siRNA against ALIX (siALIX) or a non-targeting control (siCTL) and immunostained with α-LBPA to mark late endosomes. Scale bar, 10 μm. Right: Matched lysates were immunoblotted for α-Alix. **(B)** Whole cell lysates (WCL) and exosomal fractions (Exo) from indicated cell types were resolved by SDS-PAGE and stained by Coomassie (left) or immunoblotted for exosomal markers α-Alix, α-TSG101, α-GAPDH, and α-HSC70 (right) to measure relative exosome release. Immunoblots for α-GM130 and α-PDI confirmed lack of Golgi or ER contamination in exosomal fractions. **(C)** Indicated cell types were transfected with YFP-tagged murine leukemia virus Gag (MLV Gag-YFP). Virus-like particles (VLPs) and whole cell lysates (WCL) were resolved by SDS-PAGE and immunoblotted for α-Gag to measure relative viral budding.

Figure 9

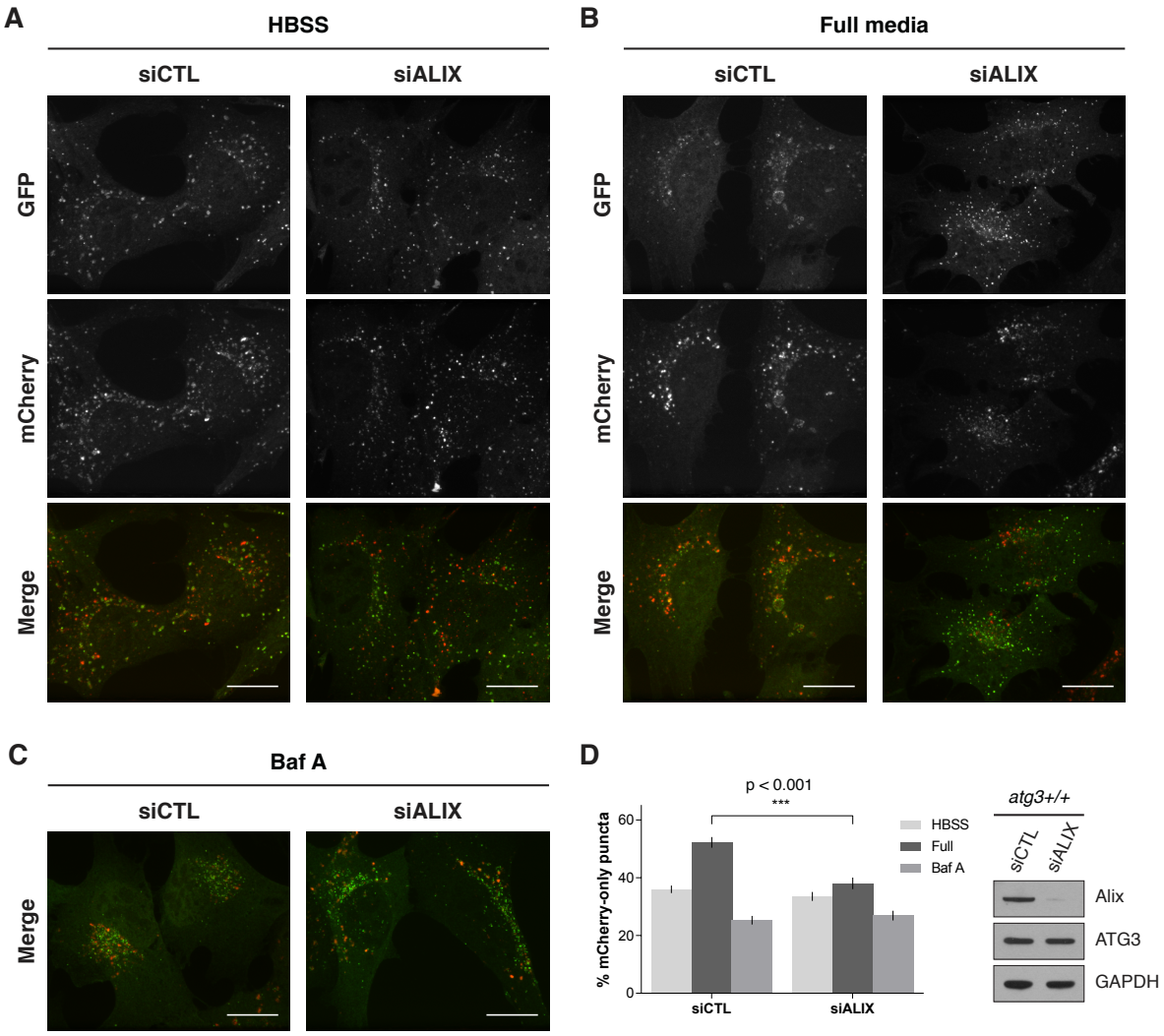
A
HBSS
siCTL
siALIX
GFP
mCherry
Merge
B
Full media
siCTL
siALIX
GFP
mCherry
Merge
C
Baf A
siCTL
siALIX
Merge
D
p < 0.001
***
% mCherry-only puncta
60
40
20
0
siCTL
siALIX
HBSS
Full
Baf A
atg3+/+
siCTL
siALIX
Alix
ATG3
GAPDH

Figure 9. Loss of Alix specifically impairs basal autophagic flux.

(A) *Atg3*$^{+/+}$ MEFs expressing mCherry-GFP-LC3 were transfected with siRNA against ALIX (siALIX) or a non-targeting control (siCTL) and HBSS starved for 2h to measure starvation-induced autophagic flux. Scale bar, 15 μm. **(B)** *Atg3*$^{+/+}$ MEFs expressing mCherry-GFP-LC3 were transfected with siALIX or siCTL and grown in full media to measure basal autophagic flux. Scale bar, 15 μm. **(C)** *Atg3*$^{+/+}$ MEFs expressing mCherry-GFP-LC3 were transfected with siALIX or siCTL and treated for 2h with Baf A (50 nM) to block lysosome function. Scale bar, 15 μm. **(D)** Left: Quantification of the percentage of mCherry-positive, GFP-negative (mCherry-only) puncta per cell for at least 100 cells from three independent experiments as described in A-C (mean ± SEM). Statistical significance calculated using ANOVA, followed by Tukey's HSD test. Right: Indicated cells were grown in full media, lysed, and immunoblotted for α-Alix.

METHODS

Reagents

Dr. Noboru Mizushima (University of Tokyo) provided *Atg5*$^{+/+}$ and *Atg5*$^{-/-}$ MEFs and Dr. Masaaki Komatsu (Tokyo Metropolitan Institute) provided *Atg3*$^{+/+}$ and *Atg3*$^{-/-}$ MEFs. Cells were cultured in DMEM with 10% fetal bovine serum (FBS), penicillin, and streptomycin.

Commercial Antibodies

Antibodies used in this study include: anti-p62 (Progen GP62-C), anti-Atg3 (Sigma A3231), anti-GAPDH (Millipore), anti-EEA1 (Cell Signaling), anti-LAMP1 (BD 553792), anti-LBPA (Echelon), anti-ATG12 (Cell Signaling 2011), anti-ATG12 (Cell Signaling 4180), anti-HA (Covance), anti-HA (Cell Signaling), anti-Alix (Cell Signaling), anti-myc (Sigma), anti-GFP (Santa Cruz), anti-phospho-ERK1/2 (Biosource), anti-ERK1/2 (Zymed), anti-phospho-AKT (Cell Signaling 2965), anti-AKT (Cell Signaling), anti-TSG101 (Abcam), anti-HSC70 (Cell Signaling), anti-GM130 (BD), anti-PDI (Cell Signaling), anti-Gag (Abcam 100970), and anti-HSP60 (Santa Cruz). A rabbit polyclonal anti-LC3 antibody was created using a peptide corresponding to the conserved N-terminal sequence of human, rat, and mouse MAP1LC3 [73] and is now commercially available (Millipore).

Microscopy

Widefield immunofluorescence imaging was performed using the 100X (1.3 NA) objective of a Zeiss Axiovert 200 microscope equipped with a Spot RT camera (Diagnostics Instruments) and mercury lamp; images were acquired using Metamorph software (Molecular Devices v6.0). Confocal analysis of mCherry-GFP-LC3 puncta in reconstituted *Atg3*$^{-/-}$ MEFs was performed using the 60X (1.4 NA) objective of a Nikon C1si spectral confocal system equipped with an

argon laser (488 line) and two solid-state diodes (405 and 546 lines); images were acquired using Nikon EZ-C1 software. All other confocal analysis was performed using the 100X (1.49 NA) objective of a Nikon inverted microscope (TE-2000 PFS) equipped with a CSU10 spinning-disk confocal unit (Yokogawa), solid-state 488 and 561 lasers, and a cooled charge-coupled device camera (Cool-SNAP-HQ2, Photometrics); images were acquired using NIS Elements software. Images were analyzed in ImageJ (v1.44i).

Immunofluorescence

For endosomal/lysosomal immunostaining, cells were fixed with 4% paraformaldehyde for 10 min at room temperature and blocked/permeabilized for 30 min at room temperature in 0.05% saponin + 10% goat serum in PBS (saponin/GS). Primary and secondary incubations were performed at room temperature in saponin/GS, and cells were mounted using Prolong Gold with or without DAPI.

Immunoblotting

Unless otherwise indicated, cells were lysed in RIPA buffer (1% Triton X-100, 1% sodium deoxycholate, 0.1% SDS, 25 mM Tris, pH 7.6, 150 mM NaCl, 10 mM NaF, 10mM β-glycerophosphate, 1 mM Na_3VO_3, 10 nM calyculin A, 0.5 mM PMSF, 0.1 mM E-64-c, 10 µg/mL pepstatin A) plus protease inhibitors. Lysates were cleared by centrifugation for 15 min at 4˚C, boiled in sample buffer, resolved by SDS-PAGE, and transferred to PVDF membrane. Membranes were blocked in 5% milk in PBS + 0.1% TWEEN 20 (PBST), incubated with primary antibodies overnight at 4˚C in blocking buffer, washed in PBST, incubated with HRP-conjugated secondary antibodies, and analyzed by enhanced chemiluminescence.

Triton fractionation

Cells were lysed in 1% Triton X-100 in PBS plus 10 mM NaF, 10 mM β -glycerophosphate, 1 mM Na_3VO_3, 10 nM calyculin A, 0.5 mM PMSF, 0.1 mM E-64-c, 10 μg/mL pepstatin A, and protease inhibitors. Lysates were incubated on ice for 30 min, and soluble and insoluble fractions were separated by centrifugation at 4˚C for 20 min at 16,000*g*. The soluble fraction was boiled in sample buffer, and the insoluble fraction was resuspended in sample buffer, sonicated, and boiled prior to immunoblotting.

Perinuclear LBPA quantification

Cells were immunostained for LBPA and DAPI and imaged by epifluorescence as described above. Images were autothresholded, and a 10 μm region of interest (ROI) around the nucleus was selected using the wand tracing and enlarge selection tools in ImageJ. The perinuclear $LBPA^+$ fraction was defined as the fraction of LBPA-positive integrated density within this ROI relative to the whole cell.

RNAi

For siRNA-mediated Alix knockdown, siGenome SMARTpool siRNAs against mouse PDCD6IP/Alix (L-062173-01) were purchased from Dharmacon RNA Technologies, and cells were transfected using an Amaxa nucleofactor apparatus (program U-020) and nucleofactor kit V according to manufacturer's instructions.

Transmission electron microscopy

Cells were pelleted for 5 min at 4 °C at 600*g*, fixed on ice for 30 min in 0.1 M sodium cacodylate buffer (pH 7.4) plus 2% glutaraldehyde and 1% PFA, and pelleted at 3,000*g* for 10 min at 4 °C.

Samples were submitted to the Gladstone Institute (UCSF) Electron Microscopy Core Facility for standard transmission electron microscopy ultrastructural analyses.

Mass Spectrometry

Lysates were immunoprecipitated with monoclonal α-HA conjugated to agarose and eluted with HA peptide (Sigma). The eluate was separated by SDS-PAGE, and Coomassie stained bands were excised, trypsin digested, and analyzed on an LTQ-Orbitrap (Thermo Fisher Scientific) located in the UCSF Mass Spectroscopy Core. Fractions were separated on a 100μm × 10 cm C18 column at flow rate 350 nL/min over a 60 min HPLC run. MS spectra were captured using one survey scan in FT at 30,000 resolution and six MS/MS events in the ion trap. Proteins were identified using Protein Prospector against the SwissProt database.

cDNAs and generation of stably reconstituted MEFs

cDNAs used in this study were previously described [1] and have been deposited with Addgene. MLV-Gag-YFP (Plasmid 1813) and mCherry-hALIX (Plasmid 21504) constructs were obtained from Addgene [74, 75]. For retroviral infection, VSV-G pseudotyped retroviruses were generated, and MEFs were infected and selected as previously described [1]. Following selection, stable pools were used at a maximum of 6-8 passages to avoid clonal selection or drift.

mCherry-GFP-LC3 autophagic flux

MEFs expressing mCherry-GFP-LC3 were grown overnight on fibronectin-coated coverslips prior to HBSS starvation or treatment with 50 nM Baf A. Cells were fixed with 4% paraformaldehyde (PFA), washed with PBS, mounted using ProLong Gold (Life Technologies), and analyzed by confocal microscopy as described in *Extended Experimental Procedures*. Following image acquisition and automatic thresholding, mCherry and GFP puncta were

quantified using the Analyze Particles plugin in ImageJ. Double-positive puncta were identified and counted using the Colocalization and Analyze Particles plugins in ImageJ.

DQ Green BSA lysosomal degradation

Cells were incubated with 20 μg/mL DQ Green BSA (DQ-BSA; Life Technologies) for 30 min at 37°C followed by a 2h chase in full media with or without 50 nM Baf A. Following treatment, cells were trypsinized, collected in cold PBS plus pepstatin A (10 μg/mL) and E-64-d (10 μg/mL) to block further degradation, and analyzed by flow cytometry using a FACSCalibur (BD) and FlowJo software.

Bodipy-LDL trafficking

Cells were serum-starved in DMEM + 0.5% BSA + 20 mM HEPES for 1h at 37°C, incubated with 10 μg/mL Bodipy FL LDL (LDL; Life Technologies) for 15 min at 37°C in serum-free media, and chased for 0, 30, or 120 min in full media. Cells were fixed in 4% PFA, immunostained for EEA1, LBPA, or LAMP1 as described in *Extended Experimental Procedures*, and analyzed by confocal microscopy. Following image acquisition and automatic thresholding, puncta were quantified using the Analyze Particles plugin in ImageJ. Colocalized puncta were identified and counted using the Colocalization and Analyze Particles plugins in ImageJ.

Transferrin uptake and recycling

Cells were serum-starved in DMEM + 0.5% BSA + 20 mM HEPES for 1h at 37°C, incubated with 25 μg/mL fluorescently labeled transferrin (Life Technologies) for 15 min at 37°C in serum-free media, and chased in full media for up to 60 min. Cells were immunostained for

EEA1 and analyzed by confocal microscopy or trypsinized, fixed in 4% paraformaldehyde, and analyzed by flow cytometry using a FACSCalibur (BD) and FlowJo software.

Lysosomal acidification and cathepsin activity

For lysosomal mass and acidification measurements, cells were incubated with 1 μM LysoSensor DND-153 or DND-189 (Life Technologies) in full media for 30 min at 37°C, trypsinized, washed in PBS, and analyzed by flow cytometry using a FACSCalibur (BD) and FlowJo software. For cathepsin activity assays, cells were trypsinized, washed in full media, incubated with Magic Red Cathepsin B or L substrates (ImmunoChemistry) for 30 min at 37°C according to the manufacturer's protocol, and analyzed by flow cytometry using a FACSCalibur (BD) and FlowJo software.

Exosome isolation

For exosome biogenesis assays, equal numbers of cells were seeded; upon reaching 80% confluence, cells were washed and incubated in equal volumes of DMEM containing 10% exosome-depleted FBS. Exosome isolation was performed 24h later by differential centrifugation as described previously [76]. The corresponding cells were lysed in RIPA as described in the *Extended Experimental Procedures*. Exosomal and whole cell lysate (WCL) fractions were resolved by SDS-PAGE and stained by Coomassie to visualize total protein or immunoblotted for exosomal and membrane markers.

Virus-like particle (VLP) isolation

For VLP budding assays, equal numbers of cells were seeded; upon reaching 80% confluence, cells were washed and incubated in equal volumes of full media. VLP isolation was performed 24h later by sequential centrifugation at 4°C. Conditioned media was spun for 5 min at 200*g* to

remove cells, filtered through a 0.45 μm pre-wet filter to remove cellular debris, overlaid on a 20% sucrose cushion and spun for 2h at 130,000*g* to pellet VLPs. The corresponding cells were lysed in RIPA, and VLP and WCL fractions were resolved by SDS-PAGE and immunoblotted with α-Gag.

Statistics

Experimental groups were compared using unpaired t test or ANOVA followed by Tukey's HSD test for multiple comparisons as indicated.

ACKNOWLEDGEMENTS

We thank Drs. Noboru Mizushima and Masaaki Komatsu for generously providing reagents. Confocal microscopy was performed in the Biological Imaging Development Center at UCSF. Grant support to J.D. includes the NIH (CA126792) and a Howard Hughes Medical Institute Physician-Scientist Early Career Award. This material is based upon work supported by the National Science Foundation Graduate Research Fellowship to LM under grant DGE-1144247.

CHAPTER 3

Autophagy and endosomal trafficking: molecular mechanisms and implications for neurodegenerative disease

Content in this chapter was modified from the following publication:

Murrow, L. & Debnath, J. Autophagy as a stress-response and quality-control mechanism: implications for cell injury and human disease. *Annual Review of Pathology* **8**, 105 (2013).

DISCUSSION

In this study, we identify roles for ATG12-ATG3 conjugation in both autophagosome maturation and late endosome function. ATG12-ATG3 conjugation controls multiple interconnected pathways, including autolysosome formation, late endosome-to-lysosome trafficking of LDL, and Alix-dependent ESCRT functions such as exosome biogenesis and viral budding. Moreover, we identify an interaction between ATG12-ATG3 and the ESCRT-associated protein Alix. Disruption of the ATG12-ATG3 complex replicates several key phenotypes associated with Alix loss-of-function, suggesting that ATG12-ATG3 promotes late endosome function via its interaction with Alix.

The endosomal and autophagy pathways are functionally connected; immature autophagosomes can fuse with MVBs in the late endocytic pathway prior to delivery to the lysosome [64, 65]. Multiple recent studies implicate components of the endosomal trafficking and vesicle fusion machineries in autophagosome maturation, including ESCRT complexes [62, 63], SNAREs [77-80], endosomal coatomers [81], and Rab GTPases [82-84]. However, little is known about whether individual ATGs functionally interact with the endosomal machinery. Importantly, our data demonstrate that ATG12-ATG3 interacts with Alix and controls MVB morphology, distribution, and function; moreover, these functions are distinct and separable from the established roles of either ATG12 or ATG3 in autophagy. This is the first study to identify a molecular interaction between components of the core autophagy and ESCRT-associated machineries. Notably, we observe defects in endolysosomal degradation in *Atg3*$^{-/-}$ and *Atg12*$^{-/-}$ MEFs, which both lack ATG12-ATG3, but see increased degradation in *Atg5*$^{-/-}$ MEFs, which lack ATG12-ATG5 yet still form ATG12-ATG3. Since all three cell types are completely

autophagy-incompetent, we conclude that the endolysosomal defects observed upon genetic loss of either ATG12 or ATG3 do not involve canonical macroautophagy.

ACTIN REMODELING DURING BASAL AUTOPHAGIC FLUX

Importantly, we show that both ATG12-ATG3 and Alix promote basal, but not starvation-induced autophagic flux. We speculate that additional signals activated during nutrient starvation bypass the requirement for these proteins in autolysosome formation. Previous studies support that homeostatic and stress-induced autophagosome maturation are functionally distinct processes. Similar to ATG12-ATG3, the histone deacetylase HDAC6 is required for basal autophagic flux but dispensable for starvation-induced autophagy [44]. HDAC6 binds ubiquitinated protein aggregates and F-actin and recruits cytoskeleton-remodeling machinery components to promote autolysosome formation at these sites. The HDAC6 substrate cortactin is required for actin remodeling at sites of protein aggregation. Loss of either HDAC6 or cortactin leads to accumulation of ubiquitinated protein aggregates and impaired autophagosome maturation under basal conditions; autophagosome maturation during starvation is unaffected by loss of either of these proteins [44].

Intriguingly, in an *in vitro* assay measuring fusion of LC3-positive autophagosomes with LAMP2-positive late endosomes or lysosomes, autophagosomes isolated from starved mouse hepatocytes retained normal fusion capacity following latrunculin treatment to block actin polymerization, whereas autophagosomes isolated from hepatocytes grown in full medium had significantly decreased fusion [44]. These data suggest that basal autophagy is uniquely dependent upon actin remodeling for autophagosome maturation whereas starvation-induced autophagy is not. One interesting possibility is that actin remodeling is essential for fusion of autophagosomes

to late endosomes but not for direct fusion to lysosomes. Starvation activates the transcription factors TFEB and TFE3, leading to coordinated expansion of the lysosomal compartment and induction of autophagy genes [85, 86]. Following this starvation-induced lysosomal biogenesis, the cell may no longer require autophagosome-endosome fusion to maintain autophagic flux.

Notably, Alix also interacts with F-actin and cortactin and is required for normal cytoskeleton organization [71, 87]. Loss of Alix in HeLa cells leads to abnormal localization of cortactin and clathrin and aberrant late endosome localization [71]. In fibroblasts, Alix promotes F-actin assembly and stress fiber formation [87]. Determining whether the interactions between ATG12-ATG3 and Alix promote autophagosome maturation through similar actin-based mechanisms is a topic for future study.

NON-CANONICAL ROLE FOR ATG12-ATG3 IN AUTOPHAGOSOME MATURATION

As discussed in Chapter 1, recent work has identified additional functions for ATGs in promoting autophagosome maturation. For example, the ATG12-ATG5 conjugate can promote autophagosome-lysosome fusion via interaction with the effector protein TECPR1 in addition to its well-established role in autophagosome elongation. [50]. Here, we identify an additional mechanism of ATG-dependent autophagosome maturation via interaction of the alternative ATG12-ATG3 conjugation product with Alix.

Although ATGs were originally identified based on their conserved role in autophagosome formation, some of these proteins may have acquired additional roles during evolution to more tightly control levels of autophagic flux and crosstalk between autophagy and other cell pathways such as endosomal trafficking. The lysine required for ATG12 conjugation is

conserved across multiple ATG3 orthologues including in *S. cerevisiae* and *A. thaliana* [1]. An interesting question for further research is identifying when during evolution the ATG12-ATG3 conjugate arose and whether its interaction with Alix orthologues is conserved.

ATG12-ATG3 PROMOTES MULTIPLE ALIX FUNCTIONS

The identification of Alix as an ATG12-ATG3 binding partner led us to scrutinize the role of ATG12-ATG3 in additional Alix-dependent functions. Alix interacts with components of the ESCRT machinery to control multiple topologically identical membrane budding events: MVB intralumenal vesicle formation [67, 68], exosome release [59], and viral budding [69, 70]. Exosome biogenesis occurs via fusion of MVBs with the plasma membrane, leading to intralumenal vesicle release as exosomes [58]. Exosomes have been identified as important signaling molecules in a wide variety of contexts, including the immune response, tumor priming of distant sites for metastasis, and transfer of mRNAs and microRNAs between cells [88-90]. Interestingly, previous work in yeast has implicated multiple ATGs in unconventional secretion of Acb1 through an exosome-like intermediate [91]. Our data identifies the ATG12-ATG3 conjugate as a novel regulator of exosome release in mammalian cells.

Viral budding is a mechanistically similar process in which late domain viral proteins interact with Alix and other ESCRT components to hijack the membrane abscission machinery [60]. Autophagy generally plays a cytoprotective role in viral infection, as xenophagy, or degradation of foreign pathogens by autophagy, is the most direct innate immune response in the cell [27]. Multiple studies have confirmed this important role for autophagy following infection. For example, autophagosomes are targeted to Sindbis virus in infected neurons, and loss of ATG5 leads to delayed viral clearance and increased cell death [92]. However, the ATG12-ATG5

conjugate also interacts with proteins such as RIG-I and IPS-1, suppressing type I interferon production and dampening the immune response [93]. Our studies suggest ATG12-ATG3 is an additional proviral ATG conjugate that promotes viral budding via its interactions with Alix.

ABERRANT AUTOPHAGY AND ENDOSOMAL TRAFFICKING IN NEURODEGENERATIVE DISEASE

Basal autophagy may be particularly important in post-mitotic cells such as neurons and myocytes because, unlike dividing cells, they are unable to dilute out damaged proteins and organelles into daughter cells [2]. Indeed, autophagy deficiency in neurons or muscle cells generally leads to atrophy and cell death [33, 34]. Neuron-specific *Atg5* and *Atg7* knockout mice develop progressive motor defects accompanied by neurodegeneration and accumulation of polyubiquitinated proteins and aggregates [33, 34]. Similarly, *Hdac6* knockout mice display age-dependent accumulation of ubiquitinated protein aggregates and neuronal cell death [44].

Given the importance of basal autophagy to normal neuron function, it is perhaps unsurprising that defects in autophagic flux are a hallmark of numerous neurodegenerative diseases including Parkinson's and Alzheimer's diseases [94]. Interestingly, Beclin 1 expression decreases with age in the human brain, suggesting that decreased autophagy may contribute to the association observed between advanced age and increased incidence of neurodegenerative disease [95].

Parkinson's disease is caused by the degeneration of dopaminergic neurons in the substantia nigra. Characteristic features of Parkinson's include accumulation of autophagic vacuoles, abnormal mitochondrial function, and the presence of Lewy bodies—intracellular inclusions containing the proteins α-synuclein and ubiquitin [94]. Studies of familial inherited

forms of Parkinson's have implicated autophagy in disease pathogenesis. Gene duplication of α-synuclein, the major component of Lewy bodies, has been observed in both familial and sporadic forms of Parkinson's disease [96, 97]. Overexpression of wild-type α-synuclein in a human neuroblastoma cell line causes mislocalization of Atg9 and suppresses autophagosome biogenesis [98]. Similarly, transgenic mice overexpressing α-synuclein accumulate abnormal autophagosomes and lysosomes in neurons, leading to progressive neurodegeneration and motor defects [99, 100]. Overall, these data suggest that impaired autophagy may underlie some aspects of α-synuclein neuropathology.

Alzheimer's disease is a form of dementia characterized by neuronal death in the cerebral cortex. The hallmarks of Alzheimer's are the presence of intracellular neurofibrillary tangles containing hyperphosphorylated tau and presence of extracellular β-amyloid (Aβ) plaques generated by cleavage of amyloid precursor protein (APP) by γ secretase [94]. Accumulation of autophagosomes and abnormal mitochondria are seen in postmortem brains of AD patients, suggesting that autophagy plays a role in disease progression [101]. Several studies suggest that defects in autophagic maturation may be a general feature of Alzheimer's pathology. Alzheimer's-associated mutations in the transmembrane protein presenilin 1 that cause a familial early-onset form of the disease lead to defects in autophagic flux due to faulty targeting of the v-ATPase V0a1 subunit to the lysosome and resulting defects in lysosomal acidification [102]. More broadly, immature forms of autophagic vacuoles such as isolation membranes and autophagosomes rather than autolysosomes accumulate in the brains of Alzheimer's patients. The accumulated autophagic vacuoles resemble those seen in primary cortical neurons following inhibition of lysosomal proteases or vinblastine treatment—both of which block autophagosome

maturation—suggesting that autophagosome accumulation in AD brains is at least partly caused by a block in autophagic flux [101, 103, 104].

At the same time, endolysosomal defects are also observed in Alzheimer's disease, and ESCRT dysfunction is associated with other neuronal pathologies including frontotemporal dementia [80, 105]. Multivesicular bodies accumulate in the brains of Alzheimer's patients in parallel with immature autophagosomes [101]. Interestingly, alterations in endosomal trafficking are observed in Alzheimer's patients before widespread Aβ accumulation occurs, suggesting that endosomal trafficking defects are fundamental to disease pathogenesis. A splice site mutation in the essential ESCRT-III component CHMP2B is associated with an inherited autosomal dominant form of frontotemporal dementia. Overexpression of mutant CHMP2B in cultured cortical neurons leads to ESCRT-III dysfunction, impaired autophagic flux, and cell death [62]. Intact ESCRT function is also required for clearance of TDP-43, the major pathogenic protein aggregate in frontotemporal dementia [61].

In this work, we have identified the ATG12-ATG3 conjugate as a novel regulator of both basal autophagy and late endosome function. A few open questions remain: Is ATG12-ATG3 conjugation constitutive, or is it regulated? How does the interaction with ATG12-ATG3 influence Alix localization or activity? Further dissecting the molecular basis and regulation of the interaction between ATG12-ATG3 and Alix may inform new therapeutic strategies for coordinately augmenting autophagosome maturation and late endosomal function in the treatment of neurodegenerative disease.

REFERENCES

1. Radoshevich, L. *et al.* ATG12 conjugation to ATG3 regulates mitochondrial homeostasis and cell death. *Cell* **142**, 590-600 (2010).
2. Mizushima, N., Levine, B., Cuervo, A.M. & Klionsky, D.J. Autophagy fights disease through cellular self-digestion. *Nature* **451**, 1069-1075 (2008).
3. Murrow, L. & Debnath, J. Autophagy as a stress-response and quality-control mechanism: implications for cell injury and human disease. *Annual Review of Pathology: Mechanisms of Disease* **8**, 105-137 (2013).
4. Klionsky, D.J. *et al.* A Unified Nomenclature for Yeast Autophagy-Related Genes. *Developmental cell* **5**, 539-545 (2003).
5. Klionsky, D.J. *et al.* Guidelines for the use and interpretation of assays for monitoring autophagy in higher eukaryotes. *Autophagy* **4**, 151 (2008).
6. Yang, Z. & Klionsky, D.J. Mammalian autophagy: core molecular machinery and signaling regulation. *Current opinion in cell biology* **22**, 124-131 (2010).
7. Ichimura, Y. *et al.* A ubiquitin-like system mediates protein lipidation. *Nature* **408**, 488-492 (2000).
8. Mizushima, N. *et al.* A protein conjugation system essential for autophagy. *Nature* **395**, 395-398 (1998).
9. Ohsumi, Y. Molecular dissection of autophagy: two ubiquitin-like systems. *Nature Reviews Molecular Cell Biology* **2**, 211-216 (2001).
10. Nemoto, T. *et al.* The mouse APG10 homologue, an E2-like enzyme for Apg12p conjugation, facilitates MAP-LC3 modification. *Journal of Biological Chemistry* **278**, 39517-39526 (2003).
11. Tanida, I. *et al.* Apg7p/Cvt2p: a novel protein-activating enzyme essential for autophagy. *Molecular biology of the cell* **10**, 1367-1379 (1999).
12. Tanida, I., Tanida-Miyake, E., Komatsu, M., Ueno, T. & Kominami, E. Human Apg3p/Aut1p homologue is an authentic E2 enzyme for multiple substrates, GATE-16, GABARAP, and MAP-LC3, and facilitates the conjugation of hApg12p to hApg5p. *Journal of Biological Chemistry* **277**, 13739-13744 (2002).
13. Kroemer, G., Mariño, G. & Levine, B. Autophagy and the integrated stress response. *Molecular cell* **40**, 280-293 (2010).
14. Rabinowitz, J.D. & White, E. Autophagy and metabolism. *Science* **330**, 1344 (2010).
15. Mizushima, N., Yamamoto, A., Matsui, M., Yoshimori, T. & Ohsumi, Y. In vivo analysis of autophagy in response to nutrient starvation using transgenic mice expressing a fluorescent autophagosome marker. *Molecular biology of the cell* **15**, 1101-1111 (2004).
16. Kuma, A. *et al.* The role of autophagy during the early neonatal starvation period. *Nature* **432**, 1032-1036 (2004).
17. Komatsu, M. *et al.* Impairment of starvation-induced and constitutive autophagy in Atg7-deficient mice. *The Journal of cell biology* **169**, 425 (2005).
18. Warr, M.R. *et al.* FOXO3A directs a protective autophagy program in haematopoietic stem cells. *Nature* **494**, 323-327 (2013).
19. Lum, J.J. *et al.* Growth factor regulation of autophagy and cell survival in the absence of apoptosis. *Cell* **120**, 237-248 (2005).
20. Roy, S. & Debnath, J. Autophagy and Tumorigenesis. *Seminars in Immunopathology* **32**, 383-396 (2010).

21. Kim, J., Kundu, M., Viollet, B. & Guan, K.L. AMPK and mTOR regulate autophagy through direct phosphorylation of Ulk1. *Nature cell biology* **13**, 132-141 (2011).
22. Hosokawa, N. *et al.* Nutrient-dependent mTORC1 association with the ULK1–Atg13–FIP200 complex required for autophagy. *Molecular biology of the cell* **20**, 1981-1991 (2009).
23. Jung, C.H. *et al.* ULK-Atg13-FIP200 complexes mediate mTOR signaling to the autophagy machinery. *Molecular biology of the cell* **20**, 1992-2003 (2009).
24. Jung, C.H., Ro, S.H., Cao, J., Otto, N.M. & Kim, D.H. mTOR regulation of autophagy. *FEBS letters* **584**, 1287-1295 (2010).
25. Mihaylova, M.M. & Shaw, R.J. The AMPK signalling pathway coordinates cell growth, autophagy and metabolism. *Nature cell biology* **13**, 1016-1023 (2011).
26. Bellot, G. *et al.* Hypoxia-induced autophagy is mediated through hypoxia-inducible factor induction of BNIP3 and BNIP3L via their BH3 domains. *Molecular and cellular biology* **29**, 2570 (2009).
27. Delgado, M. *et al.* Autophagy and pattern recognition receptors in innate immunity. *Immunological reviews* **227**, 189-202 (2009).
28. Ebato, C. *et al.* Autophagy is important in islet homeostasis and compensatory increase of beta cell mass in response to high-fat diet. *Cell metabolism* **8**, 325-332 (2008).
29. Jung, H.S. *et al.* Loss of Autophagy Diminishes Pancreatic [beta] Cell Mass and Function with Resultant Hyperglycemia. *Cell metabolism* **8**, 318-324 (2008).
30. Masiero, E. *et al.* Autophagy is required to maintain muscle mass. *Cell metabolism* **10**, 507-515 (2009).
31. Nakai, A. *et al.* The role of autophagy in cardiomyocytes in the basal state and in response to hemodynamic stress. *Nature medicine* **13**, 619-624 (2007).
32. Raben, N. *et al.* Suppression of autophagy in skeletal muscle uncovers the accumulation of ubiquitinated proteins and their potential role in muscle damage in Pompe disease. *Human molecular genetics* **17**, 3897 (2008).
33. Hara, T. *et al.* Suppression of basal autophagy in neural cells causes neurodegenerative disease in mice. *Nature* **441**, 885-889 (2006).
34. Komatsu, M. *et al.* Loss of autophagy in the central nervous system causes neurodegeneration in mice. *Nature* **441**, 880-884 (2006).
35. Kraft, C., Peter, M. & Hofmann, K. Selective autophagy: ubiquitin-mediated recognition and beyond. *Nature cell biology* **12**, 836-841 (2010).
36. Kirkin, V. *et al.* A role for NBR1 in autophagosomal degradation of ubiquitinated substrates. *Molecular cell* **33**, 505-516 (2009).
37. Pankiv, S. *et al.* p62/SQSTM1 binds directly to Atg8/LC3 to facilitate degradation of ubiquitinated protein aggregates by autophagy. *Journal of Biological Chemistry* **282**, 24131-24145 (2007).
38. Geisler, S. *et al.* PINK1/Parkin-mediated mitophagy is dependent on VDAC1 and p62/SQSTM1. *Nature cell biology* **12**, 119-131 (2010).
39. Deosaran, E. *et al.* NBR1 acts as an autophagy receptor for peroxisomes. *Journal of cell science* **126**, 939-952 (2013).
40. Thurston, T.L., Ryzhakov, G., Bloor, S., von Muhlinen, N. & Randow, F. The TBK1 adaptor and autophagy receptor NDP52 restricts the proliferation of ubiquitin-coated bacteria. *Nature immunology* **10**, 1215-1221 (2009).

41. von Muhlinen, N., Thurston, T., Ryzhakov, G., Bloor, S. & Randow, F. NDP52, a novel autophagy receptor for ubiquitin-decorated cytosolic bacteria. *Autophagy* **6**, 288-289 (2010).
42. Wild, P. *et al.* Phosphorylation of the autophagy receptor optineurin restricts Salmonella growth. *Science* **333**, 228-233 (2011).
43. Kawaguchi, Y. *et al.* The deacetylase HDAC6 regulates aggresome formation and cell viability in response to misfolded protein stress. *Cell* **115**, 727-738 (2003).
44. Lee, J.Y. *et al.* HDAC6 controls autophagosome maturation essential for ubiquitin-selective quality-control autophagy. *The EMBO journal* **29**, 969-980 (2010).
45. Rubinstein, A.D., Eisenstein, M., Ber, Y., Bialik, S. & Kimchi, A. The Autophagy Protein Atg12 Associates with Antiapoptotic Bcl-2 Family Members to Promote Mitochondrial Apoptosis. *Molecular cell* **44**, 698-709 (2011).
46. Zhao, Z. *et al.* Autophagosome-independent essential function for the autophagy protein Atg5 in cellular immunity to intracellular pathogens. *Cell Host & Microbe* **4**, 458-469 (2008).
47. Reggiori, F. *et al.* Coronaviruses Hijack the LC3-I-positive EDEMosomes, ER-derived vesicles exporting short-lived ERAD regulators, for replication. *Cell Host & Microbe* **7**, 500-508 (2010).
48. Bestebroer, J., V'kovski, P., Mauthe, M. & Reggiori, F. Hidden behind autophagy: the unconventional roles of ATG proteins. *Traffic* **14**, 1029-1041 (2013).
49. Subramani, S. & Malhotra, V. Non-autophagic roles of autophagy-related proteins. *EMBO reports* **14**, 143-151 (2013).
50. Chen, D. *et al.* A mammalian autophagosome maturation mechanism mediated by TECPR1 and the Atg12-Atg5 conjugate. *Molecular cell* **45**, 629-641 (2012).
51. Liang, C. *et al.* Beclin1-binding UVRAG targets the class C Vps complex to coordinate autophagosome maturation and endocytic trafficking. *Nature cell biology* **10**, 776-787 (2008).
52. Matsunaga, K. *et al.* Two Beclin 1-binding proteins, Atg14L and Rubicon, reciprocally regulate autophagy at different stages. *Nature cell biology* **11**, 385-396 (2009).
53. Zhong, Y. *et al.* Distinct regulation of autophagic activity by Atg14L and Rubicon associated with Beclin 1–phosphatidylinositol-3-kinase complex. *Nature cell biology* **11**, 468-476 (2009).
54. Raiborg, C. & Stenmark, H. The ESCRT machinery in endosomal sorting of ubiquitylated membrane proteins. *Nature* **458**, 445-452 (2009).
55. Katzmann, D.J., Odorizzi, G. & Emr, S.D. Receptor downregulation and multivesicular-body sorting. *Nature Reviews Molecular Cell Biology* **3**, 893-905 (2002).
56. Mellman, I. Endocytosis and molecular sorting. *Annual review of cell and developmental biology* **12**, 575-625 (1996).
57. Fevrier, B. & Raposo, G. Exosomes: endosomal-derived vesicles shipping extracellular messages. *Current opinion in cell biology* **16**, 415-421 (2004).
58. Théry, C., Zitvogel, L. & Amigorena, S. Exosomes: composition, biogenesis and function. *Nature Reviews Immunology* **2**, 569-579 (2002).
59. Baietti, M.F. *et al.* Syndecan-syntenin-ALIX regulates the biogenesis of exosomes. *Nature cell biology* **14**, 677-685 (2012).
60. Martin-Serrano, J. & Neil, S.J. Host factors involved in retroviral budding and release. *Nature Reviews Microbiology* **9**, 519-531 (2011).

61. Filimonenko, M. *et al.* Functional multivesicular bodies are required for autophagic clearance of protein aggregates associated with neurodegenerative disease. *The Journal of cell biology* **179**, 485-500 (2007).
62. Lee, J.-A., Beigneux, A., Ahmad, S.T., Young, S.G. & Gao, F.-B. ESCRT-III dysfunction causes autophagosome accumulation and neurodegeneration. *Current biology* **17**, 1561-1567 (2007).
63. Rusten, T.E. *et al.* ESCRTs and Fab1 regulate distinct steps of autophagy. *Current biology* **17**, 1817-1825 (2007).
64. Berg, T.O., Fengsrud, M., Stromhaug, P.E., Berg, T. & Seglen, P.O. Isolation and characterization of rat liver amphisomes - Evidence for fusion of autophagosomes with both early and late endosomes. *Journal of Biological Chemistry* **273**, 21883-21892 (1998).
65. Fader, C.M., Sanchez, D., Furlan, M. & Colombo, M.I. Induction of autophagy promotes fusion of multivesicular bodies with autophagic vacuoles in k562 cells. *Traffic* **9**, 230-250 (2008).
66. Kimura, S., Noda, T. & Yoshimori, T. Dissection of the autophagosome maturation process by a novel reporter protein, tandem fluorescent-tagged LC3. *Autophagy* **3**, 452-460 (2007).
67. Katoh, K. *et al.* The ALG-2-interacting protein Alix associates with CHMP4b, a human homologue of yeast Snf7 that is involved in multivesicular body sorting. *Journal of Biological Chemistry* **278**, 39104-39113 (2003).
68. Matsuo, H. *et al.* Role of LBPA and Alix in multivesicular liposome formation and endosome organization. *Science* **303**, 531-534 (2004).
69. Segura-Morales, C. *et al.* Tsg101 and Alix interact with murine leukemia virus Gag and cooperate with Nedd4 ubiquitin ligases during budding. *Journal of Biological Chemistry* **280**, 27004-27012 (2005).
70. Strack, B., Calistri, A., Craig, S., Popova, E. & Göttlinger, H.G. AIP1/ALIX is a binding partner for HIV-1 p6 and EIAV p9 functioning in virus budding. *Cell* **114**, 689-699 (2003).
71. Cabezas, A., Bache, K.G., Brech, A. & Stenmark, H. Alix regulates cortical actin and the spatial distribution of endosomes. *Journal of cell science* **118**, 2625-2635 (2005).
72. Petiot, A. *et al.* Alix differs from ESCRT proteins in the control of autophagy. *Biochemical and biophysical research communications* **375**, 63-68 (2008).
73. Fung, C., Lock, R., Gao, S., Salas, E. & Debnath, J. Induction of autophagy during extracellular matrix detachment promotes cell survival. *Molecular biology of the cell* **19**, 797-806 (2008).
74. Sherer, N.M. *et al.* Visualization of retroviral replication in living cells reveals budding into multivesicular bodies. *Traffic* **4**, 785-801 (2003).
75. Lee, H.H., Elia, N., Ghirlando, R., Lippincott-Schwartz, J. & Hurley, J.H. Midbody targeting of the ESCRT machinery by a noncanonical coiled coil in CEP55. *Science* **322**, 576-580 (2008).
76. Théry, C., Amigorena, S., Raposo, G. & Clayton, A. Isolation and characterization of exosomes from cell culture supernatants and biological fluids. *Current Protocols in Cell Biology*, 3.22. 21-23.22. 29 (2006).
77. Moreau, K., Ravikumar, B., Renna, M., Puri, C. & Rubinsztein, D.C. Autophagosome precursor maturation requires homotypic fusion. *Cell* **146**, 303-317 (2011).

78. Nair, U. *et al.* SNARE proteins are required for macroautophagy. *Cell* **146**, 290-302 (2011).
79. Itakura, E., Kishi-Itakura, C. & Mizushima, N. The hairpin-type tail-anchored SNARE syntaxin 17 targets to autophagosomes for fusion with endosomes/lysosomes. *Cell* **151**, 1256-1269 (2012).
80. Lu, Y., Zhang, Z., Sun, D., Sweeney, S.T. & Gao, F.-B. Syntaxin 13, a Genetic Modifier of Mutant CHMP2B in Frontotemporal Dementia, Is Required for Autophagosome Maturation. *Molecular cell* **52**, 264-271 (2013).
81. Razi, M., Chan, E.Y. & Tooze, S.A. Early endosomes and endosomal coatomer are required for autophagy. *The Journal of cell biology* **185**, 305-321 (2009).
82. Gutierrez, M.G., Munafó, D.B., Berón, W. & Colombo, M.I. Rab7 is required for the normal progression of the autophagic pathway in mammalian cells. *Journal of cell science* **117**, 2687-2697 (2004).
83. Jäger, S. *et al.* Role for Rab7 in maturation of late autophagic vacuoles. *Journal of cell science* **117**, 4837-4848 (2004).
84. Ganley, I.G., Wong, P.-M., Gammoh, N. & Jiang, X. Distinct autophagosomal-lysosomal fusion mechanism revealed by thapsigargin-induced autophagy arrest. *Molecular cell* **42**, 731-743 (2011).
85. Martina, J.A. *et al.* The Nutrient-Responsive Transcription Factor TFE3 Promotes Autophagy, Lysosomal Biogenesis, and Clearance of Cellular Debris. *Science signaling* **7**, ra9 (2014).
86. Settembre, C. *et al.* TFEB links autophagy to lysosomal biogenesis. *Science* **332**, 1429-1433 (2011).
87. Pan, S. *et al.* Involvement of the conserved adaptor protein Alix in actin cytoskeleton assembly. *Journal of Biological Chemistry* **281**, 34640-34650 (2006).
88. Bobrie, A., Colombo, M., Raposo, G. & Théry, C. Exosome secretion: molecular mechanisms and roles in immune responses. *Traffic* **12**, 1659-1668 (2011).
89. Hood, J.L., San, R.S. & Wickline, S.A. Exosomes released by melanoma cells prepare sentinel lymph nodes for tumor metastasis. *Cancer research* **71**, 3792-3801 (2011).
90. Valadi, H. *et al.* Exosome-mediated transfer of mRNAs and microRNAs is a novel mechanism of genetic exchange between cells. *Nature cell biology* **9**, 654-659 (2007).
91. Duran, J.M., Anjard, C., Stefan, C., Loomis, W.F. & Malhotra, V. Unconventional secretion of Acb1 is mediated by autophagosomes. *The Journal of cell biology* **188**, 527-536 (2010).
92. Orvedahl, A. *et al.* Autophagy protects against Sindbis virus infection of the central nervous system. *Cell Host & Microbe* **7**, 115-127 (2010).
93. Jounai, N. *et al.* The Atg5–Atg12 conjugate associates with innate antiviral immune responses. *Proceedings of the National Academy of Sciences* **104**, 14050 (2007).
94. Cheung, Z.H. & Ip, N.Y. Autophagy deregulation in neurodegenerative diseases – recent advances and future perspectives. *Journal of neurochemistry* **118**, 317-325 (2011).
95. Shibata, M. *et al.* Regulation of intracellular accumulation of mutant Huntingtin by Beclin 1. *Journal of Biological Chemistry* **281**, 14474 (2006).
96. Ross, O.A. *et al.* Genomic investigation of α-synuclein multiplication and parkinsonism. *Annals of neurology* **63**, 743-750 (2008).
97. Ahn, T.-B. *et al.* α-Synuclein gene duplication is present in sporadic Parkinson disease. *Neurology* **70**, 43-49 (2008).

98. Winslow, A.R. *et al.* α-Synuclein impairs macroautophagy: implications for Parkinson's disease. *The Journal of cell biology* **190**, 1023-1037 (2010).
99. Masliah, E. *et al.* Dopaminergic loss and inclusion body formation in α-synuclein mice: implications for neurodegenerative disorders. *Science* **287**, 1265 (2000).
100. Spencer, B. *et al.* Beclin 1 gene transfer activates autophagy and ameliorates the neurodegenerative pathology in α-synuclein models of Parkinson's and Lewy body diseases. *The Journal of Neuroscience* **29**, 13578-13588 (2009).
101. Nixon, R.A. *et al.* Extensive involvement of autophagy in Alzheimer disease: an immuno-electron microscopy study. *Journal of Neuropathology & Experimental Neurology* **64**, 113 (2005).
102. Lee, J.H. *et al.* Lysosomal proteolysis and autophagy require presenilin 1 and are disrupted by Alzheimer-related PS1 mutations. *Cell* **141**, 1146-1158 (2010).
103. Boland, B. *et al.* Autophagy induction and autophagosome clearance in neurons: relationship to autophagic pathology in Alzheimer's disease. *The Journal of Neuroscience* **28**, 6926-6937 (2008).
104. Yu, W.H. *et al.* Macroautophagy—a novel β-amyloid peptide-generating pathway activated in Alzheimer's disease. *The Journal of cell biology* **171**, 87-98 (2005).
105. Nixon, R.A. Endosome function and dysfunction in Alzheimer's disease and other neurodegenerative diseases. *Neurobiology of aging* **26**, 373-382 (2005).

Publishing Agreement

It is the policy of the University to encourage the distribution of all theses, dissertations, and manuscripts. Copies of all UCSF theses, dissertations, and manuscripts will be routed to the library via the Graduate Division. The library will make all theses, dissertations, and manuscripts accessible to the public and will preserve these to the best of their abilities, in perpetuity.

Please sign the following statement:

I hereby grant permission to the Graduate Division of the University of California, San Francisco to release copies of my thesis, dissertation, or manuscript to the Campus Library to provide access and preservation, in whole or in part, in perpetuity.

Author Signature

9/8/2014
Date